AES/PE/13-34 **Foam Stability in Presence of Oil: A Simulation and Experimental study**

30/08/2013 **Ahmed Amir Abdulkereem Hussain**

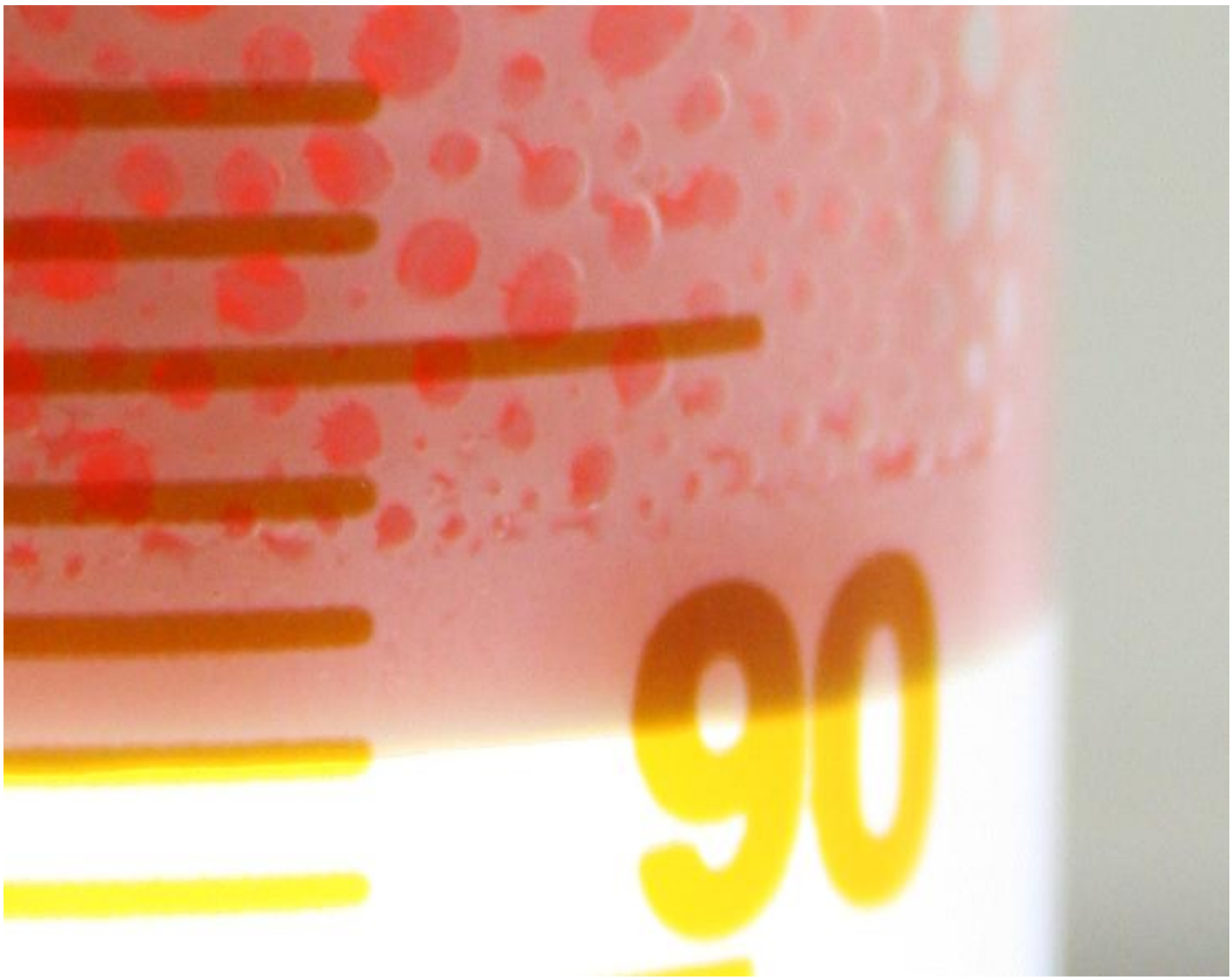

TU Delft Delft University of Technology

Challenge the future

Title	:	Foam Stability in Presence of Oil: A Simulation and Experimental Study
Author(s)	:	Ahmed Amir Abdulkereem Hussain
Date	:	August 2013
Professor(s)	:	Dr. William R. Rossen
Supervisor(s)	:	Dr. Rouhollah Farajzadeh and Dr. Sébastien Vincent-Bonnieu
TA Report number	:	AES/PE/13-34

Postal Address	:	Section for Petroleum Engineering Department of Geoscience & Engineering Delft University of Technology P.O. Box 5028 The Netherlands
Telephone	:	(31) 15 2781328 (secretary)
Telefax	:	(31) 15 2781189

Executive summary

This thesis investigates bulk foam stability in absence of oil, and in presence of oil (hexadecane). Foam in absence of oil was produced by sparging nitrogen at a fixed flow rate through the surfactant solution. Foam in presence of oil was produced by stirring a mixture of surfactant and oil with an immersion mixer. The behavior of foam in absence of oil did not give any prediction of the behavior of foam in the presence of oil. We show that commonly referred methods for foam stability in presence of oil, the entering, spreading, and bridging coefficients and lamella number, did not give reliable predictions. The surfactants that produced most stable foams in presence of oil had the lowest interfacial tension with oil. We also show that in our experiments, foam in presence of oil does not show a relationship between foam bubble diameter and drainage rate, unlike foam in absence of oil. We illustrate that foam in presence of oil, produced with a mixture of surfactants, can be more stable than the foams in presence of oil, which were produced with the individual surfactants. We observed emulsions forming under foam in presence of oil, and their maximum volumes have not shown any relationship with other parameters.

This thesis also investigates foam injection into a water-flooded reservoir by a single cycle surfactant-alternating-gas (SAG) mode. We demonstrate that if not enough surfactant is injected into the reservoir, the oil bank (ahead of the foam front) does not reach the production well. Therefore less oil is produced, since less gas is injected due to foam reducing the injectivity of gas. We show the effect of oil on the foam front stability. In our simulations foam collapses in gridblocks where oil saturation is above a certain threshold value. The liberated gas flows upward in the reservoir, and pushes down oil and water. This can result in the formation of an oil bank at the bottom of the reservoir, and in our simulations this oil bank is not displaced by foam because its oil saturation is high enough to destroy foam. We varied the threshold value of minimum water saturation for stable foam; if the threshold is set at a larger value (reflecting less stable foam), then foam has a less significant impact on oil production and gas injection than if it is set at a lower threshold value (reflecting more-stable foam).

Acknowledgement

I offer my sincerest gratitude to my thesis supervisors Prof. Bill Rossen and to Dr. Rouhi Farajzadeh for their constant and invaluable guidance. They introduced me to such an interesting topic and providing me an opportunity to work at Shell Global Solutions International B.V., Rijswijk.

I have been indebted in the preparation of this thesis to Dr. Sébastien Vincent-Bonnieu, who has supported me throughout my thesis with his patience and knowledge whilst allowing me the room to work in my own way.

I am very much grateful to Dr. Alexey Andrianov for his guidance and generous help in performing reservoir simulations, and sharing his knowledge.

I also express my thankfulness to Dr. Ali Fadili, Adi Anand, Bart Wassing, Prof. George Hirasaki, Dr. Hans Groot, Dr. Leon Kapetas, Nikita Lenchenkov, and Rahul Thorat for their valuable inputs throughout this thesis.

I wish to appreciate all the members of the Dietz lab that contributed through good advice and their good spirits to this thesis. Many thanks go to Arno, Dik, Ellen, Henk, Jan, Jolanda, Karel, Michiel, and Wim. I would also like to thank Dr. Hua Guo for helping me with setting up the experiments with the FoamScan.

In addition, I am grateful to the committee members of my MSc defense for reviewing my thesis and giving valuable comments.

I would like to express my deepest thanks to my family. I am extremely thankful to my parents for their love and blessings, and for their patience in these years. I am grateful to my brothers, who were always my main source of motivation.

List of abbreviations

C_s	Surfactant concentration in aqueous phase	[kg/kg]
C_s^*	Critical surfactant concentration for foam stability	[kg/kg]
epdry	Regulates the F_w function near *fmdry*	[-]
epoil	Parameter in F_o dependence on S_o	[-]
epsurf	Parameter in F_s dependence on C_s	[-]
floil	Lower oil saturation (volume fraction) for the effect of oil on foam	[m^3/m^3]
fmdry	Critical water saturation (volume fraction) for foam stability	[m^3/m^3]
fmmob	Reference value of mobility-reduction factor at maximum foam strength	[-]
fmoil	Critical oil saturation (volume fraction) for foam stability	[m^3/m^3]
F_o, F_w, F_s	Functions describing the effects of oil or water phase saturations or surfactant concentration, respectively, on foam stability	[-]
k	Permeability	[Darcy]
$k_{r\alpha}$	Relative permeability of Phase α	[-]
$k^0_{r\alpha}$	Endpoint relative permeability of Phase α	[-]
MRF	Mobility reduction factor	[-]
n	Drainage rate	[-]
n_α	Corey exponent of Phase α	[-]
p_{wf}	Well bottomhole pressure	[Pa]
P_{red}	Reference pressure in reservoir	[Pa]
S_α	Saturation of Phase α	[m^3/m^3]
S^*_α	Critical saturation of Phase α (either water or oil)	[m^3/m^3]
S_{α_r}	Residual saturation of Phase α	[m^3/m^3]
S_{org}	Residual oil saturation to gas flood	[m^3/m^3]
S_{orw}	Residual oil saturation to water flood	[m^3/m^3]
t_{end}	Duration of simulation	[days]
t_{gas}	Duration of gas-injection period	[days]
t_s	Switching time; duration of surfactant-injection period	[days]
λ^f_{rg}	Gas relative mobility in presence of foam (ratio of relative permeability and viscosity)	[1/Pa·s]
λ^{nf}_{rg}	Gas relative mobility in presence of foam (ratio of relative permeability and viscosity)	[1/Pa·s]
μ	Viscosity	[Pa·s]
ϕ	Porosity	[m^3/m^3]

Subscripts

Cum	Cumulative
g	Gas phase
inj	Injected
max	Maximum
min	Minimum
o	Oil phase
w	Water phase
α	Water/oil/gas phase

Superscripts

*	Critical
f	In the presence of foam
inj	Injection well
nf	In the absence of foam
prod	Production well

Table of contents

List of figures

List of tables

1. Introduction

1.1. Gas flooding EOR

Producing a hydrocarbon reservoir by its natural energy will result in a large fraction of the initial hydrocarbon in place to be left behind in the reservoir. Consequently, it is desirable to extract the remaining oil by injecting other fluids into the reservoir. Gas flooding is one of the widely used methods of enhanced oil recovery (EOR) [1]. It is the injection of hydrocarbon (mixture of methane to propane), or non-hydrocarbon (carbon dioxide, nitrogen, flue gas, steam, and hydrogen sulfide) components into oil reservoirs, that usually have been water flooded to residual oil saturation [2]. The main advantage of gas flooding is the low residual oil saturation, which occurs due to its good microscopic sweep efficiency compared to water flooding [3]. Gas can reduce the viscosity, and swell the oil phase upon mixing, and can lower the interfacial tension between oil and the displacing phase, specially under miscible conditions. Gas floods are commonly divided into miscible floods and immiscible floods. For miscible gas floods the injected gas dissolves into the oil, and forms a single phase. This could be achieved by injecting CO_2 or light hydrocarbons at high pressures. For immiscible gas floods the injected gas partially dissolves into the oil and the capillary force is still considerable.

The unfavorable mobility ratio in gas EOR process, combined with the reservoir heterogeneity, can form a major hurdle [4, 5] and result in a poor volumetric sweep efficiency, leaving a large fraction of oil untouched by the injected gas. This can happen due to gas flowing in the high permeability streaks (which might occur in heterogeneous reservoirs), and viscous fingering can occur due to the viscosity difference between the oil and the gas, or gas can override the oil due to the large density contrast between the injected gas and in-situ liquids [4-6].

Foam can drastically reduce the mobility of the gas phase by creating liquid films blocking the gas flow and/or by trapping a large gas fraction inside the porous medium [7]. The latter effect reduces the gas relative permeability by blocking some of the gas flow paths [2]. Therefore, foaming of the injected gas is a potential solution to the aforementioned challenges in gas EOR processes [8, 9]. Foam can also be used to support thermal or chemical EOR processes [10-13].

1.2. Foam EOR

Foam is gas dispersed in a continuous liquid phase. The gas pockets are separated from each other by thin liquid films called lamellae [14]. The surfactant molecules are present at the gas-liquid interface, and thereby stabilize the foam films [15]. Foam can substantially hinder gas flow in porous media, which forces gas to sweep pores that it would not have reached without foam [16]. The two main methods to obtain foam in porous media are co-injection of gas and surfactant, and alternating injection of surfactant and gas slugs (SAG) [16, 17]. Bond and Holbrook [18] were the first to propose the use of foam for gas mobility control, after which several successful field applications (in pilot scale) of foam have followed. Some examples are the East Vacuum field in the USA, and the Oseberg field and the Snorre field offshore Norway [10, 13, 19, 20]. It was found that the gas mobility was reduced by a greater factor in the relatively high permeable layers than in the relatively low permeable layers. Thereby, part of the gas entered the low permeable layers, which had not been swept up to then, resulting in an improvement in both vertical and areal sweep efficiency.

Up to now, most of the modeling and experimental studies have been devoted to describe the behavior of foam in the absence of oil, and relatively few studies on foam in the presence of oil have been performed [2]. It is not fully understood how stability of foam and its

propagation in reservoirs is affected by oil. Published researches on bulk foam and full-field simulations indicate that the presence of oil can severely affect the success of foam-flood performance [2, 16, 21]. The understanding of the impact of oil on foam generation, propagation, and destruction is essential to develop a solid foam process for any given field where oil is present. Published research on this subject shows a disagreement on the ability of foam to generate and propagate when oil is present (in porous media). Some research indicate that the presence of oil can be unfavorable on foam stability, while other research indicates that relatively stable foam can be formed in the presence of oil [17, 22-25]. Some propose that foam cannot be formed above a certain critical value of oil saturation, while others have found that foam can be generated at relatively high oil saturations [9, 17, 21, 26]. In some studies it was found that the type of oil was not crucial for foam generation and propagation, rather the type of surfactant exhibited large effects, while others found the foaming behavior to depend upon the combination of surfactant and oil types [8, 17, 27, 28].

1.3. Objectives of the thesis

The main objective of this research is to achieve a better understanding of foam-oil interaction by performing systematic bulk foam studies and reservoir simulations. More specifically, the objectives of this thesis are as follows:

- Surfactant screening; identifying surfactants that generate stable bulk foam in the presence of hexadecane.
- Investigating the parameters of bulk foam stability in the presence of oil.
- Demonstrate that oil has significant impact on foam stability and foam front propagation in a SAG process.
- Describe how foam front propagation and oil production depends upon the injected surfactant volume in a SAG process.
- Demonstrate the impact of the threshold water saturation, below which foam is unstable, in a SAG process.

1.4. Outline of the thesis

The thesis consists of 3 chapters, starting with Chapter 1 as the introduction.

Chapter 2 deals with the systematic study to screen surfactants. The foaming properties of a selected set of commercially available surfactants used in the petroleum industry are investigated in the absence of oil, and in presence of oil (hexadecane). Bulk foam in absence of oil is generated by sparging nitrogen at a fixed flow rate through the surfactant solution. Bulk foam in presence of oil is generated by stirring the mixture with an immersion mixer. Effect of surfactant type and hexadecane are investigated by measuring the foam volume, liquid fraction of foam, and bubble diameter of foam. These data are used to explain the dominating destruction mechanisms during foam decay in the absence and presence of hexadecane. The results of this chapter will serve as a basis for future surfactant screening by core-flood experiments. We end this chapter with our conclusions and recommendations for further study.

In chapter 3 we investigate surfactant-alternating-gas (SAG) injection in reservoir simulations. The reservoir is homogeneous and initially the reservoir is saturated only with water and oil, and the oil saturation is defined to be residual after water flooding, in every gridblock. Surfactant and gas injection rate are a function of the pressure difference between the injection well and reservoir, similarly the production rate is a function of pressure difference between the production well and reservoir. The surfactant injection period is variable, and the gas injection period is fixed at 250 days. We look at the cumulative oil, and gas production per simulation. We investigate the water, gas, and oil saturation, and gas viscosity in gridblocks at the end of the simulations. We also show the surfactant concentration in gridblocks after surfactant injection and after gas injection. We end this chapter with our conclusions, and recommendations for further study.

2. Bulk foam stability in absence and presence of oil

A systematic laboratory study of foamability and foam stability is reported. Foam was generated by sparging nitrogen gas at a fixed flow rate of 16 ml/min through the surfactant solution in the absence of hexadecane. In the presence of hexadecane, foam was generated by stirring the surfactant solution mixed with hexadecane with an immersion mixer. We examined the foaming properties of a selected set of commercial surfactants used in the petroleum industry. It was found that properties of bulk foam in absence of oil did not give reliable predictions on the behavior of bulk foam in the presence of hexadecane. The relation between bubble diameter and the rate of liquid drainage of foam in absence of oil did not hold for foam in presence of hexadecane. The obtained results for foam stability in the presence of oil were discussed in terms of the classical entering/spreading coefficient, oil emulsification, drainage rate, bubble diameter, and initial foam volume.

2.1. Introduction

Surfactants (**surf**ace **act**ive **a**ge**nts**) are compounds consisting of a part which has affinity for non-polar media and a part that has affinity for polar media. The molecules form oriented mono-layers at interfaces and lower the surface or interfacial tension of the medium in which they are dissolved. Surfactants are sometimes defined as molecules capable of forming micelles. A surfactant molecule has a hydrophilic head group and a hydrophobic chain (or tail), see **Figure 1**. The head group usually interacts strongly with an aqueous environment and is solvated by dipole-dipole or ion-dipole interactions [29]. The head group sits in the water phase and the tail points towards the non-polar phase (e.g. air or oil), and thereby the surfactant lowers the surface tension, σ. This is due to the following reason: because water molecules at the surface have fewer bonds with surrounding water molecules than internal water molecules, an associated excess energy exists, which minimizes the surface area, this is the surface tension. The surfactant molecules lower the excess energy of missing bonds, and thereby they lower the surface tension. A surfactant generates the lowest surface tension when the surface is maximally covered by surfactant molecules; the concentration above which this occurs is known as the critical micelle concentration (*CMC*). Above the CMC micelles start to form [15].

Surfactants are divided into categories based upon the nature of the polar head group. The head group of an anionic surfactant is negatively charged, and that of a cationic surfactant is positively charged. A nonionic surfactant has a head group which does not carry a net charge [29]. Zwitterionic and amphoteric surfactants have a heads with two oppositely charged groups. Zwitterionic surfactants are not affected by the pH of the solution. An amphoteric surfactant changes its behavior from cationic to zwitterionic, and finally to net anionic as the pH increases [30].

Surfactant adsorption may occur due to electrostatic interaction, van der Waals interaction, hydrogen bonding, and/or solvation and desolvation of adsorbate and adsorbent species [29]. Cationic surfactants can alter the wettability of swelling-clays into oil-wet [29].

In this research experiments were performed on surfactants that have been successfully applied in pilots and/or have shown positive results in published research papers.

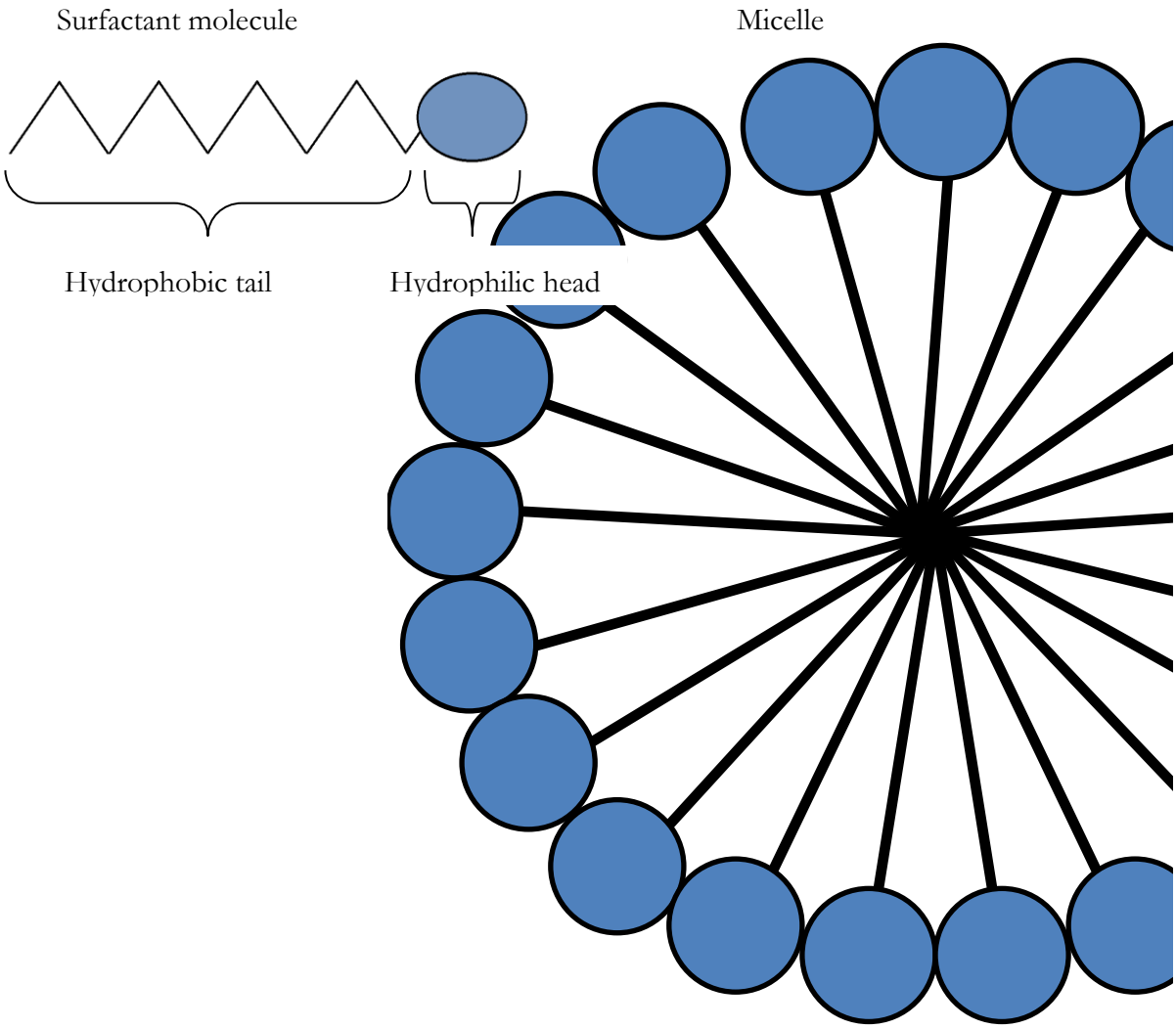

Figure 1: Schematic drawing of a surfactant molecule and a micelle.

2.1.1. General bulk foam stability theory

Foams consist of gas bubbles trapped in a liquid or a solid. In our research the liquid is water, which contains surfactant and electrolyte (NaCl). Thin foam films consist of two monolayers of surfactant molecules, with the aqueous phase in between. The repulsive forces between the surfactant monolayers cause static stability. The charged groups at the interface will cause an electrostatic repulsive force between ionic surfactants. For nonionic surfactants static stability is achieved by the overlap of hydrophobic tails which cause steric repulsion [15].

Foams stays stable for a finite period of time. There are three (interlinked) mechanisms that contribute to the destabilization and finally destruction of foam; the three mechanisms are: coarsening, liquid drainage and collapse.

Coarsening is the diffusion of gas from one gas bubble to another bubble. The pressure over the gas liquid interface can be described by Laplace's formula. The Laplace formula states that the pressure difference between gas inside the bubble, and liquid outside of the bubble, is inversely related to the bubble radius (*R*) see **Eq.(1)**, therefore the pressure in smaller bubbles is higher than in larger bubbles, and therefore gas will flow from relative small bubbles to large bubbles. Liquid drainage is the following phenomenon: liquid that is situated between the foam films and in the plateau borders will flow downward due to gravity and due to capillary suction in the plateau borders. Over time, foam bubbles will have less liquid between each other

and thus come closer to each other.

Collapse is the phenomenon of two bubbles merging when in contact to form a single foam bubble.

$$P_c = P_{gas} - P_{liq} = \frac{2\sigma}{R} \; for \; spherical \; bubbles \qquad (1)$$

Figure 2 shows three gas bubbles, with lamellae between them and a Plateau border. The pressure in the lamella is different from the plateau border because the two surfaces of the foam film interact with each other more due to their proximity to each other. Proximity of ions with similar charges and steric effects will cause repulsive forces. Attractive van der Waals forces will play a role as well [16]. The repulsive force per unit area is represented as a pressure to be included in the equilibrium condition and is known as the disjoining pressure (Π) [14]. The pressure difference across the gas-liquid interface is the capillary pressure, see **Eq. (2)**. In equilibrium the capillary pressure is equal to the disjoining pressure, see **Eq. (3)**.

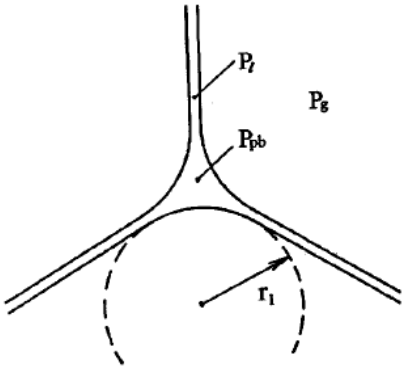

Figure 2: Illustration of three similar gas bubbles, lamellae between two bubbles (pressure = P_l), and a Plateau border (pressure = P_{pb} = P_{liq}), from Kornev et al. [31].

$$P_c = P_{gas} - P_{liq} \quad \textbf{(2)}$$

$$\Pi(\mathrm{h}) = \Pi_{\mathrm{EL}} + \Pi_{\mathrm{VW}} = P_c, in\ equilibrium \quad \textbf{(3)}$$

The van der Waals component of the disjoining pressure has a negative sign in symmetric foam films. In asymmetric films the contribution of Π_{VW} can be positive and therefore this force can be attractive or repulsive. If $\Pi_{EL} > \Pi_{VW} + P_C$ the film surfaces are well apart, and thus the foam film and the foam are stable. If the negative component of Π is stronger (i.e. $\Pi_{EL} < \Pi_{VW} + P_C$), the two foam film surfaces are in contact, and the films collapse and the foam is unstable [16].

The disjoining pressure can be obtained experimentally. The obtained disjoining pressure curve can be described with the Derjaguin-Landau-Verwey-Overbeek (DLVO) theory. The DLVO theory combines electrostatic forces, which tend to stabilize the films, and van der Waals forces, which tend to destabilize the foam film. The thickness of the foam film can then be determined by the balance between the disjoining pressure and the external pressure applied on the film [32]. **Figure 3** gives an illustration of typical disjoining pressure isotherms. Π_c is the critical disjoining pressure, at which rupture will take place.

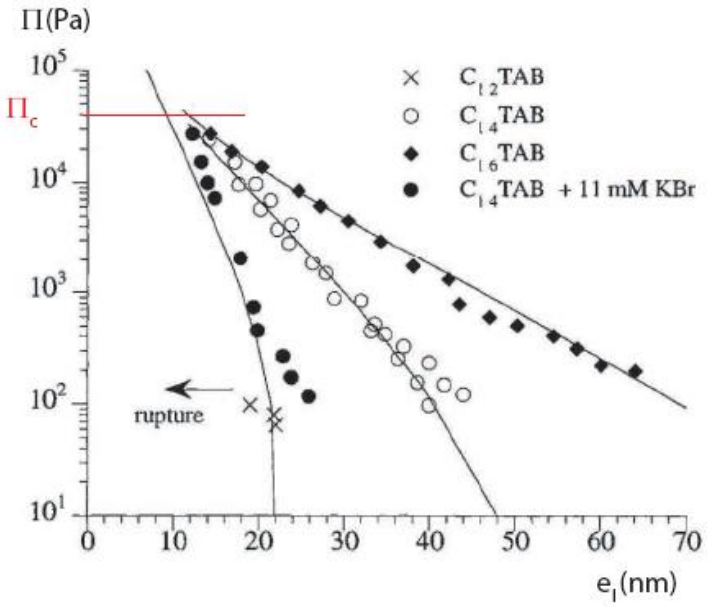

Figure 3: This figure shows an example of disjoining pressure vs. film thickness. These were measured with C_nTAB surfactant solutions. Π_c denotes the critical disjoining pressure. Adapted from Bergeron et al. [33].

2.1.1.1. Liquid fraction evaluation

Local liquid fraction of the foam can be obtained from conductivity measurements, which are made by the FoamScan (a foaming device, to be discussed in paragraph 2.2.2.2, "Foaming in absence of oil"), and the average liquid fraction of the foam column can be calculated with the foam volume and liquid volume, see **Eq. (4)** .

$$\varepsilon = \frac{V_{\text{liquid in foam}}}{V_{\text{foam}}} \qquad \textbf{(4)}$$

The normalized liquid fraction, see **Eq. (5)**, is used in this research to compare results from different experiments.

$$\varepsilon_{\text{norm}} = \frac{\varepsilon}{\varepsilon_{\text{initial}}} \qquad \textbf{(5)}$$

Where $\varepsilon_{initial}$ is the liquid fraction after the foaming process is concluded. Saint-Jalmes et al. [34] found that the liquid fraction of foam follows a power law with respect to time, see **Eq. (6)**. The constant n is referred to as the drainage rate in this report. The dimensionless drainage rate gives information on the flow regime, and it holds $2 > n > 1$ for mobile (plug-like flow) and $1 > n > 2/3$ for immobile (Poiseuille flow) surfaces [34-36]. **Figure 4** gives an illustration of the typical behavior of normalized liquid fraction of foam as a function of time. In this report the drainage rate is estimated over the period for which it has the highest value, while the foam is not collapsing.

$$\log \varepsilon_{\text{norm}} = -n \cdot \log t \qquad \textbf{(6)}$$

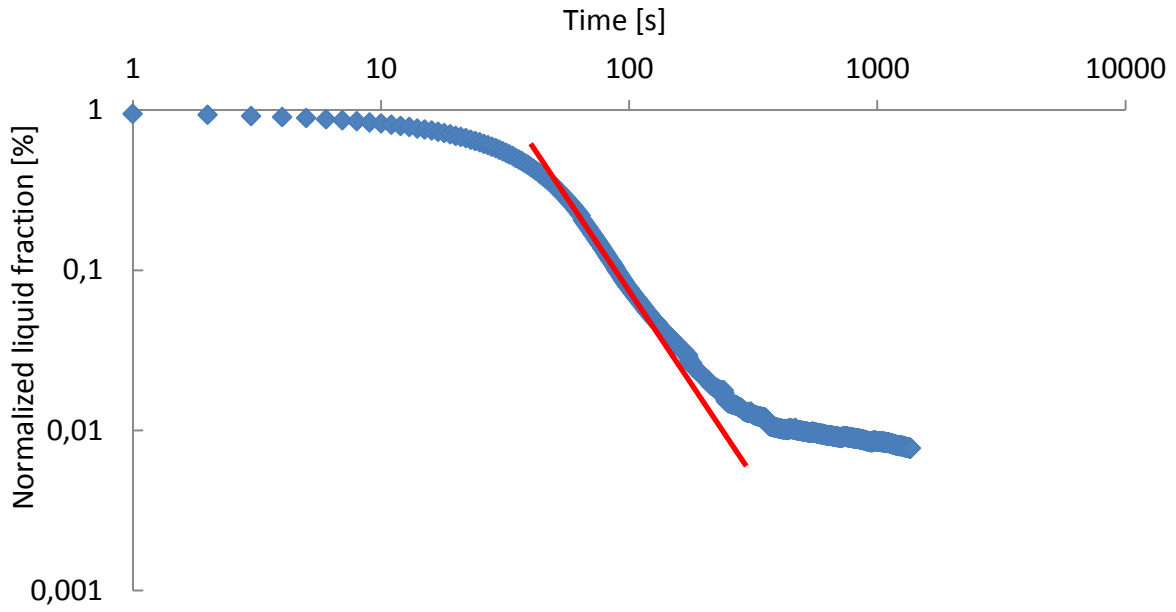

Figure 4: This figure shows an example of the normalized liquid fraction as a function of time in our bulk foam experiments. The red line is drawn parallel to the normalized liquid fraction over the period in which the drainage rate is estimated.

2.1.2. Bulk foam stability in presence of oil

When foam is injected into hydrocarbon formations to improve the oil recovery, it will come in presence of oil. The stability of foam in the presence of oil is a major concern for foam to be a good mobility control agent as it needs to stay stable when it comes in presence of oil [2, 16]. Research has shown that oil with low molecular weight is more detrimental to foam stability than oil with a high molecular weight [8, 21, 37-39]. However, systematic foam tests to explain the reason behind this phenomenon are missing [40]. Some studies report that stable foams can be achieved while in presence of oil by selecting suitable foaming agents. Other research [23] has shown that a hydrocarbon surfactant can reduce the effective viscosity of gas greater in presence of oil than without oil. They also showed that adding fluorinated surfactant to hydrocarbon surfactant can increase the foam tolerance to oil. The stability of foam in presence of oil is improved by increasing the length of the hydrophobic chain length of the hydrocarbon surfactant , which increases its solubilizing power for hydrocarbons [27].

Several models to predict foam stability have been proposed, but there is not a model that will hold under any scenario of foam in presence of oil [16, 40]. Therefore for a field application of foam we perform an extensive surfactant screening.

2.1.2.1. Models of bulk foam stability in presence of oil

The "Bridging-Spreading" mechanism is commonly used to predict foam stability when in presence of oil [2, 16, 40, 41]. The entering coefficient, $E_{o/w}$ (see **Eq. (7)**) describes the feasibility of an oil droplet to enter the gas-water interface.

$$E_{o/w} = \sigma_{wg} + \sigma_{ow} - \sigma_{og} \quad \textbf{(7)}$$

If $E_{o/w} < 0$, the oil droplet will remain in the aqueous phase and thus the foam will be stable. It is thermodynamically favorable for the oil droplet to enter the gas-water interface if $E_{o/w} > 0$.

The spreading coefficient, $S_{o/w}$ (see **Eq. (8)**), evaluates the feasibility of spreading of an oil droplet over the gas-water interface. If the spreading coefficient and the entering coefficient are positive, the oil droplet spreads over the gas-water interface, and the gas-water interface might expand, resulting in thinning of the foam film and possibly rupturing because of that.

$$S_{o/w} = \sigma_{wg} - (\sigma_{ow} + \sigma_{og}) \quad \textbf{(8)}$$

If the oil droplet enters the gas-water interface, but does not spread, the bridging coefficient (*B*), see **Eq. (9)**, describes if the water will move away from the oil drop. If the bridging coefficient is positive, a capillary pressure will occur in the foam film, which will force the water to move away from the oil drop. The oil drop enters both surfaces of the lamella, i.e. the droplet forms an unstable bridge across the foam film. For negative values of the bridging coefficient, the spreading coefficient is negative as well, see **Eq. (8)**, thus spreading, and bridging will not take place.

$$B = \sigma_{wg}^2 + \sigma_{ow}^2 - \sigma_{og}^2 \quad \textbf{(9)}$$

The "Briding-Spreading" mechanism is summarized in **Table 1**.

E / S	-	+	
		B	
-	Stable foam	-	+
		Stable foam	Unstable foam
+	Stable foam	Unstable foam	

Table 1: Foam stability prediction by the sign of the entering, spreading, and bridging coefficient, adapted from Simjoo [2].

Another proposed mechanism for predicting foam stability incorporates oil emulsification and imbibitions in the foam structure [42, 43]. If small oil droplets are formed by emulsification, they will be able to move to the inside of the foam structure. The ratio of the capillary suction in the Plateau border (**Eq. (10)**) to the capillary pressure across the oil-water interface (**Eq. (11)**) is the dimensionless *Lamella number* (**Eq. (12)**)[42].

The capillary suction in the Plateau border draws oil into lamella where a pinch-off mechanism produces emulsified oil, see **Eq.(10)**, where r_p is equal to the radius of the Plateau border.

$$\Delta p_c = \frac{2\sigma_{wg}}{r_p} \qquad \textbf{(10)}$$

The pressure difference across an oil-water interface is shown in **Eq. (11)**, where r_o is the radius of curvature of the oil surface.

$$\Delta p_R = \frac{2\sigma_{ow}}{r_o} \qquad \textbf{(11)}$$

The *Lamella number*, see **Eq. (12)**, is a dimensionless number that gives an indication of the foam stability. It is the ratio of Δp_c and Δp_R. The foam will be stable for a lamella number smaller than one, semi-stable for values between one and seven, and unstable for values larger than seven [42]. Schramm and Novosad [42, 43] found that r_o/r_p was equal to 0.15 in their experiments. In this research we will assume the ratio is 0.15 as well; due to the extensive use of this value in research papers, it has achieved benchmarking power [2, 23, 37, 44, 45].

$$L = \frac{\Delta p_c}{\Delta p_R} = \frac{r_o}{r_p}\frac{\sigma_{wg}}{\sigma_{ow}} \qquad \textbf{(12)}$$

2.2. Experimental description

2.2.1. Material and methods

The foaming experiment was performed on several surfactant solutions. The surfactants that were used in our experiments are kept confidential, and only their hydrophilic-head charges are given in this report, see **Table 2**. In this report the surfactants will be referred to by their reference names listed in **Table 2**. The surfactants were not treated after they were received. The surfactant solutions were prepared using a brine, containing 3 wt% sodium chloride in de-mineralized water (**pH=6.8±0.1)**. The surfactant concentrations were chosen as 0.5 wt% active content, which is well above the critical micelle concentration of all surfactants. The investigated surfactant mixtures and their surfactant concentrations are given in **Table 3**; the surfactants are assumed to be completely soluble in the solutions.

Reference	Charge	CMC (mg/l)	Molar weight g/mol
Surf 1	Anionic	1.03E+00	332
Surf 2	Amphoteric	1.72E+03	201
Surf 3	Anionic	2.20E+01	324
Surf 4	Zwitterionic	3.17E-02	360
Surf 5	Nonionic	Does not create micelles	186
Surf 6	Anionic	2.20E+1	324
Surf 7	Zwitterionic	3.17E-02	360
Surf 8	Anionic	1.03E+00	332

Table 2: This table gives the references of the surfactants used in the experiments, with their charge, CMC, molar weight.

Surfactant solutions	Concentrations (wt %)
Surf 1	0.5
Surf 2	0.5
Surf 3	0.5
Surf 3 + Surf 4	0.25 + 0.25
Surf 4	0.5
Surf 4 + Surf 5	0.38 (Surf 4) +0.12 (Surf 5)
Surf 6	0.5
Surf 7	0.5
Surf 8	0.5

Table 3: This table shows the investigated surfactant mixtures. The mixture Surf 3 + Surf 4 consisted for 0.25 wt% of surfactant 3, and 0.25 wt% of surfactant 4. The mixture Surf 4 + Surf 5 consisted for 0.38 wt% of surfactant 4 and 0.12 wt% of surfactant 5.

Hexadecane ($_nC_{16}$) was used to investigate the effect of oil on foam stability. **Table 4** gives some of the chemical and physical properties of hexadecane. We used 50 ppm of oil-soluble red dye (oil red O, by Sigma-Aldrich) to dye the oil, which helped us visualize the oil in the foam and surfactant solution. The dye does not have an influence on the behavior of foam, when in presence of oil [2]. All the measurements and tests are carried out at atmospheric pressure and at ambient temperature (19±1 °C) unless mentioned otherwise.

Purity	Density at 20 °C (g/cm^3)	Molecular weight (g/mol)	Viscosity (mPa·s)	API gravity (°API)	Surface tension at 20 °C mN/m)
95%	0.77	226.44	3.454	52.27	27.47

Table 4: Physical and chemical properties of the hexadecane used in this research [46-48].

2.2.2. Experimental set-up

2.2.2.1. Surface- and interfacial-tension measurements

Interfacial and surface tensions were measured with a KSV Sigma 700 tensiometer, using the du Noüy ring method. All measurements were performed at 19±1 °C and atmospheric pressure, with an average of 5 measurements per surfactant. The investigated solutions were in 100 mL uncontaminated beakers. Reference measurements were performed on demineralized water.

The force required to pull a platinum wire ring off the interface is related to the interfacial tension [49]. The ring is fully submerged in the solution and subsequently raised upwards. As the ring reaches the interface, it raises a meniscus of the liquid which will eventually tear. The force required to pull up the wire ring along with meniscus can be used to calculate the surface or interfacial tension. If the measurement is performed on an aqueous solution, the wire ring is carefully rinsed with de-mineralized water and dried with a soft tissue. If the experiment is performed on an oily liquid or suspension the wire ring is carefully degreased with acetone, and then heated with a torch.

2.2.2.2. Foaming in absence of oil

The FoamScan instrument (Teclis, France), shown in **Figure 5**, was used to find the foaming and stability properties of the surfactants. To generate foam, nitrogen gas was used with a purity of **99.98**% (less than 0.5 ppm O_2). By injecting the nitrogen gas through a porous glass frit, the foam was generated. The nitrogen gas was sparged at a fixed flow rate (16±1 cm^3/min) in a surfactant solution which contained the same initial volume for all experiments (50±1 cm^3).

During the foaming process, when the foam volume becomes equal to the target value of 100 cm^3, the gas flow will stop automatically. The top of the foam column was determined by a CCD camera. Due to the mechanical limitations of the instrument, the gas flow does not stop immediately after the foam volume limit is reached; the foam volume will thus become slightly larger than 100 cm^3.

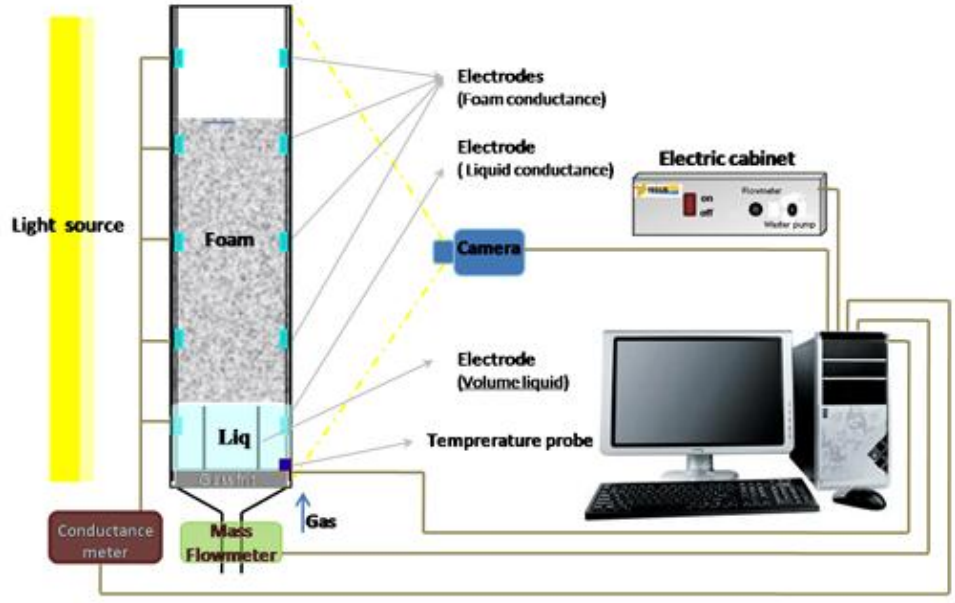

Figure 5: Schematic depiction of the FoamScan setup. Camera determined the top of the foam, and the amount of liquid volume was obtained from the conductivity data.

The following parameters were measured in the FoamScan set-up: foam volume generated during gas sparging (foamability), decay of foam volume after gas sparging (foam stability) and the water saturation in the foam. The foam capacity (FC) and the foam maximum density (MD) coefficients describe the foamability of the surfactant solution. The ratio of the foam volume at the end of the gas sparging to the total gas volume injected is the FC coefficient. If the injected gas is not retained in the foam column, it means the foam is not stable during the foaming process and the FC coefficient is less than unity, and is considered to have a poor foamability. The MD coefficient is equal to the ratio of the liquid fraction in the foam to the foam volume, which describes the liquid retention in the generated foam.

The local liquid fraction of the foam is calculated by conductivity measurements made by the electrodes at four different heights of the foam column. The electrodes can measure conductivity of foam in the interval 200 000 – 1 μSiemens, and have an accuracy of 1 μSiemens. This method has been used to measure liquid fraction of foams, and it can accurately measure liquid fractions as low as 10^{-5} [50].

Electrodes at the bottom of the column are used for the calibration of the conductivity of the liquid, from which the liquid height is calculated.

A Charged-Coupled Device (CCD) camera determines the top of foam column. The foam volume is calculated by using the height of the foam column and the height of the liquid column.

To determine the bubble diameter at a fixed level in the column, we took pictures of the foam during the experiment, see **Figure 6**. The interval at which we took the pictures depended upon the stability of the foam.

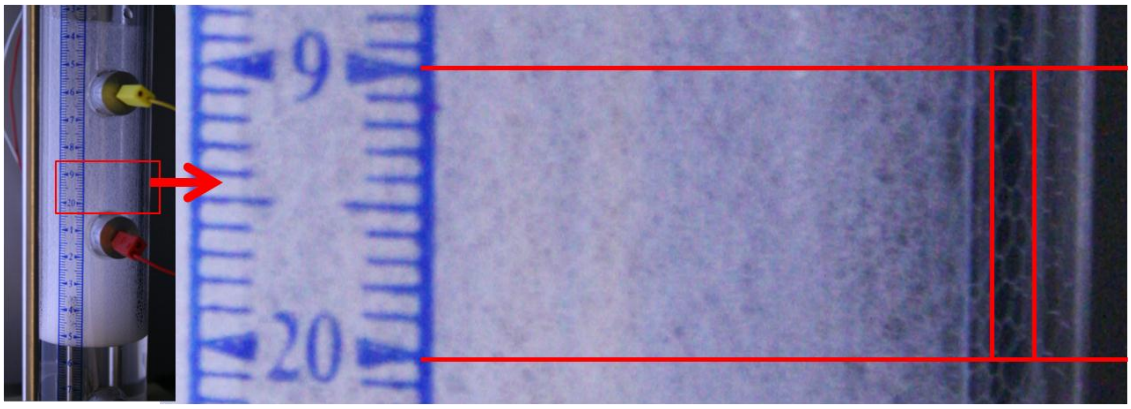

Figure 6: This illustration shows how the bubble diameter was estimated at a fixed level in the column. In the red box, the bubbles stack up to 1 cm, and are counted to get an estimation of the bubble diameter.

During each experiment we measured the top and the bottom of the foam column, from which the foam volume and the liquid volume were calculated. These values were used to check the FoamScan data.

The experiments were stopped at either half-time (when the foam is less than half of the initial volume, i.e. 50 cm^3), or when the FoamScan recorded a foam volume which differed more than 20% from the manual measurements.

2.2.2.3. Foaming in presence of oil

Due to the technical limitations of the FoamScan device, we could not use the device to perform foam stability experiments in presence of oil. Therefore we chose to use an immersion mixer to create foam in a "wide glass column", which had a diameter of 6.684 cm. We prepared 100 grams surfactant solution, and 5±0.25 cm^3 oil in the column, see **Figure 7**. We used the Philips HR1615/00 immersion mixer to create the foam, by stirring at maximum speed for 30 seconds. After the foaming process, the foam is poured into a "slim glass column", which had a diameter of 3.082 cm, and thus has a smaller tolerance (1 cm^3, compared to 10 cm^3 for the "wide glass column").

A paper ruler was taped to the "slim glass column", because the grid on the column does not give a reading below 30 cm^3.

While mixing the solution, and while pouring the foam from the "wide glass column" to the "slim glass column", part of the solution was spilled. For every experiment we weighed the solutions before and after the experiment, to measure the weight of the solution on which the experiment was performed. For some experiments this measurement was not performed and we took the average of the measurements for further calculations (100.5 grams surfactant + oil). For liquid fraction calculations we assumed a density of 1 g/cm^3.

All the experiments were performed twice, one in the presence of dyed oil and one in the presence of un-dyed oil.

During the experiment we measured the top and the bottom of the foam column, from which the foam volume and the liquid volume were calculated, and made photographs. Some of the photographs were used to determine the bubble diameter of the foam at a certain level in the column, at a fixed moment after the foaming process is concluded. The measurements were performed simultaneously, and the intervals at which the measurements were performed depended upon the stability of the foam. We stopped the experiments at half-time, i.e. when the foam volume was half the initial foam volume.

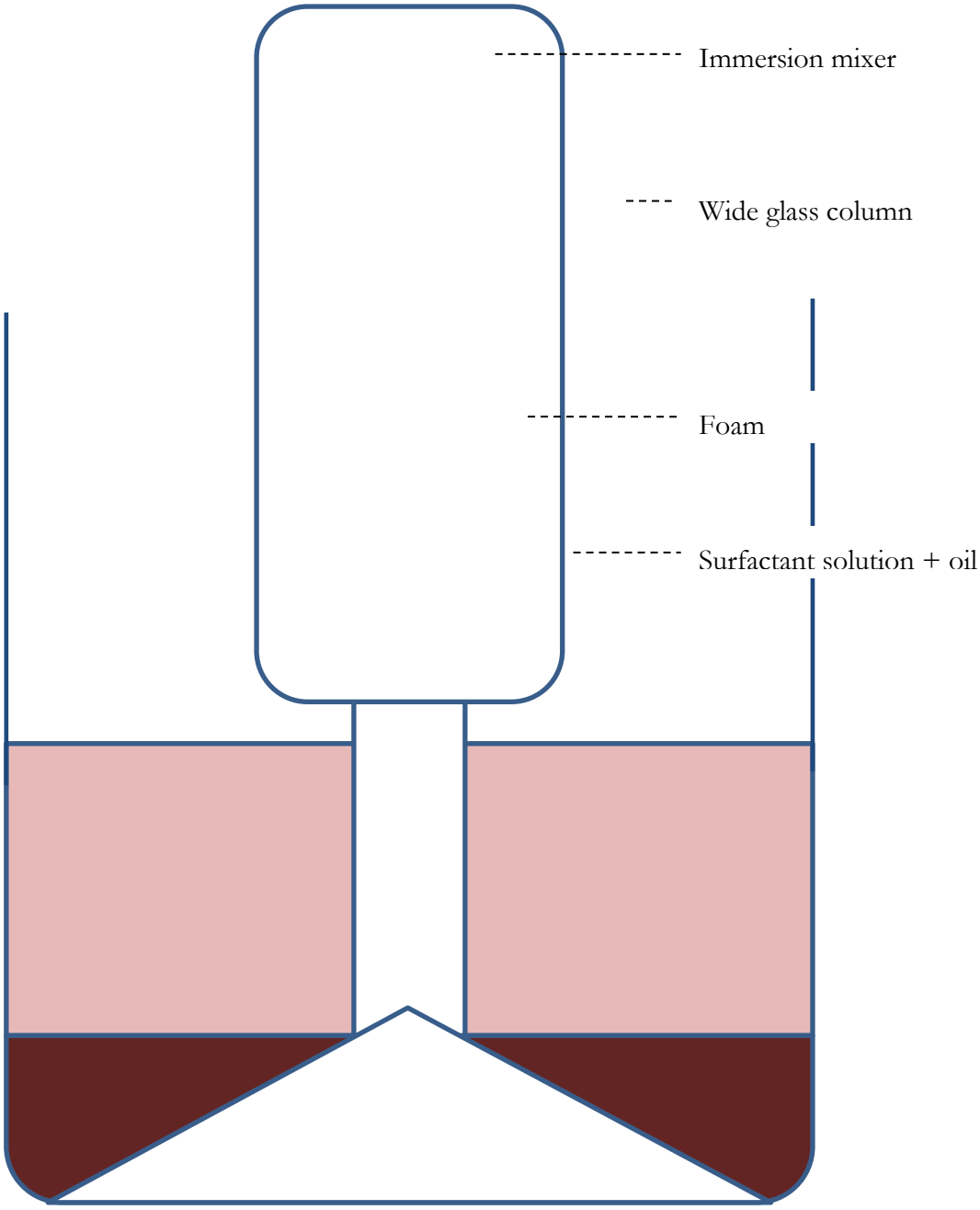

Figure 7: Schematic depiction of the foaming process of the foam in presence of oil (not to scale).

2.3. Results and discussions

2.3.1. Bulk foam in absence of oil

Foams are considered to be more stable when the foam volume remains unchanged for longer time. The foam stability is quantified by the half-life time, which is the time at which after the creation of the foam, half of the foam volume has collapsed. **Figure 8** gives the foam volume measurements of the second experiment performed on Surf 4. The foam volume is automatically measured by the FoamScan, and measured manually periodically. It shows that after a certain

period the FoamScan measurements become incorrect. This is due to the liquid fraction of the foam; the top of the foam cannot be detected by the camera of the FoamScan if the foam is too dry. The experiments were stopped when the foam measurements were 20% off the manual measurements, and their half-times were set to 10000 seconds. In the first part of the experiment, the FoamScan seems to overestimate the foam volume. This difference is not due to the liquid fraction of the foam as the foam has a high liquid fraction initially and the conductivity measurements work nominally. Notably, the illumination is not as intense as it ought to be; therefore the contrast of the camera image was increased. This may have changed the volume measurements. However the validity of the measurements is acceptable, at least for comparison, because the error is systematically the same for all surfactants. **Figure 9** gives the half-times of the foams.

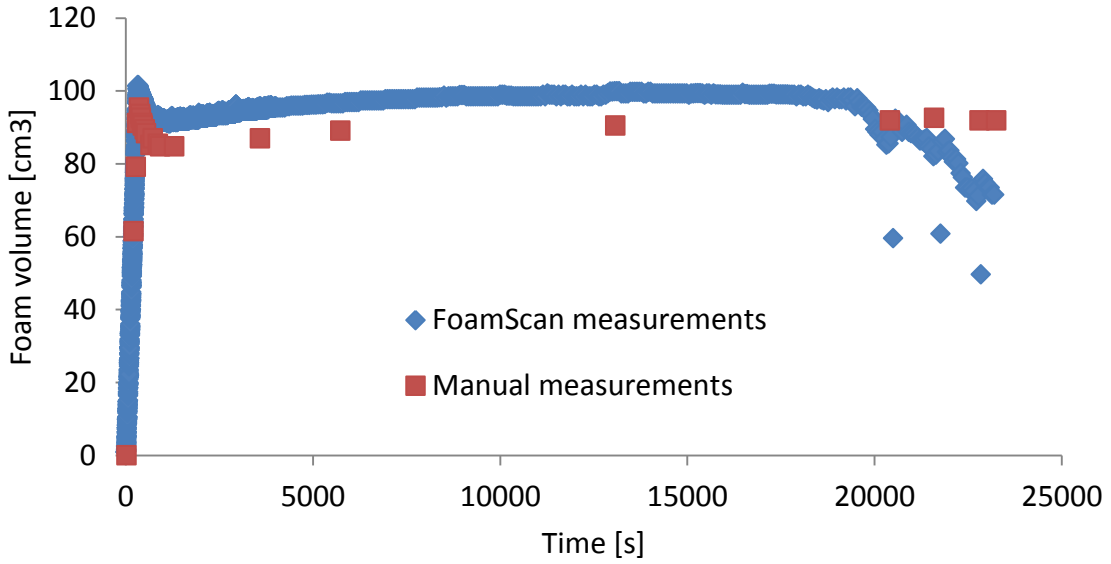

Figure 8: This figure gives the foam volume measurements of the second experiment performed on surfactant 4. It shows that after a certain period in time the FoamScan measurements become incorrect.

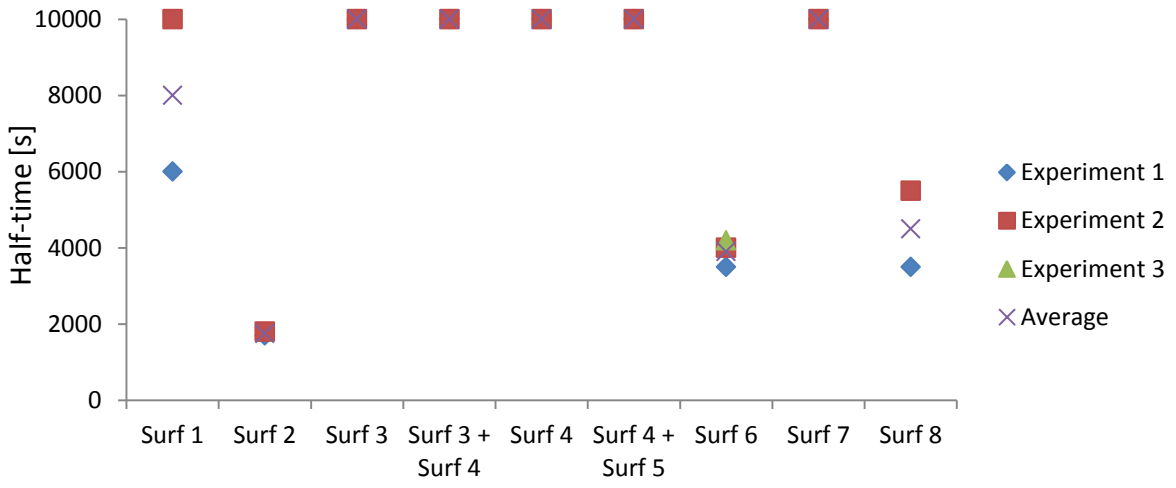

Figure 9: This figure illustrates the half time for the different experiments, which were manually checked. The experiments were stopped after 10000 seconds due to inaccuracy of the apparatus.

The drainage rate indicates how fast liquid drains out of foam, as described in section 2.1.1.1. **Figure 10**

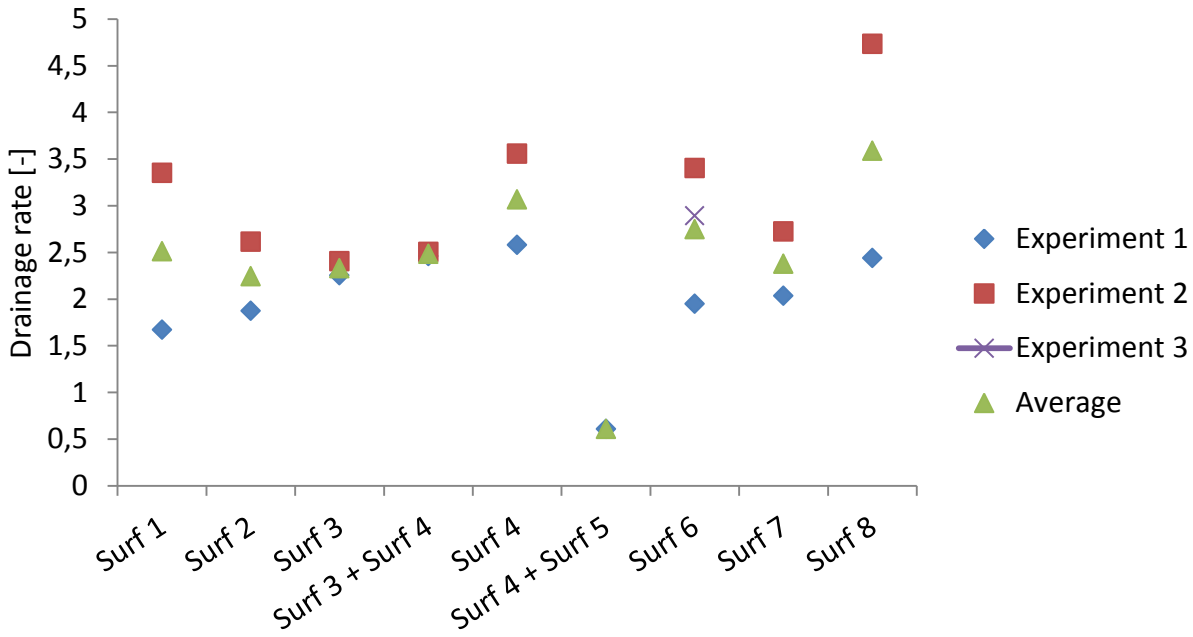

gives the drainage rate of the foams. The figure shows that the drainage rate of the foams were not reproducible (only a single experiment was performed on the mixture of surfactant 4 and surfactant 5). This figure shows that the drainage rate of foam Surf 4 + Surf 5 is 0.5, and the other foams have a drainage rate of about 2.5. Not all of the surfactant was dissolved in the mixture Surf 4 + Surf 5, see **Figure 11**. Because not all the surfactant is dissolved, and the mixture is not homogeneous, the behavior of the foam cannot be assumed to be similar to that of the other foams, which were made out of homogenous solutions.

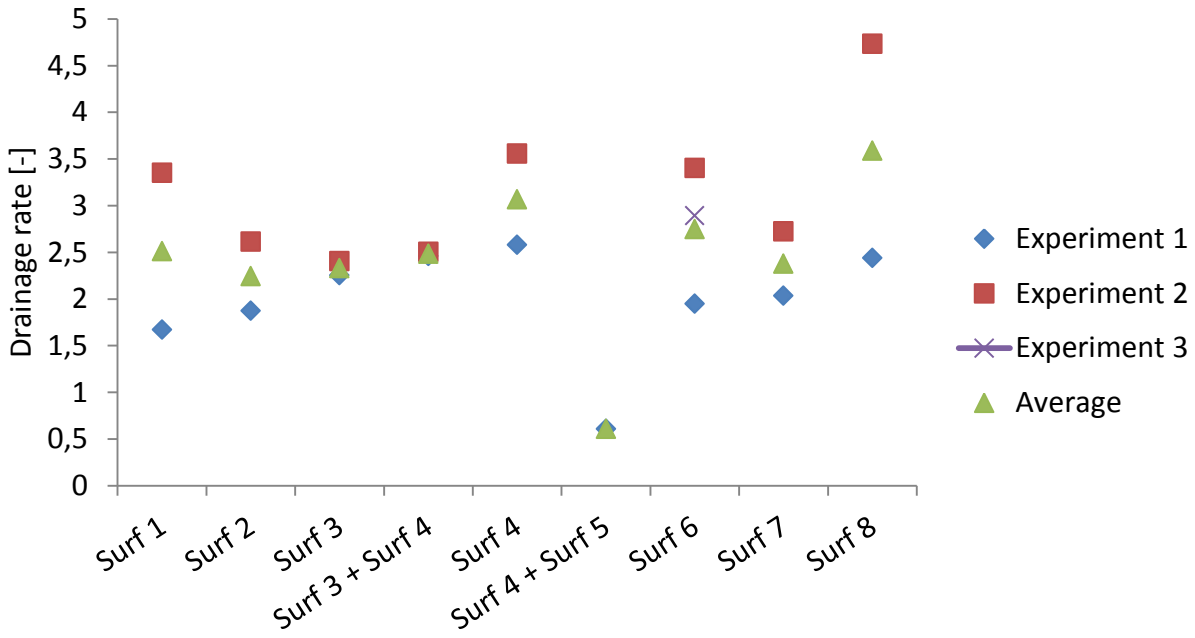

Figure 10: This figure shows the drainage rates that were found for individual experiments and their average. The drainage rate was obtained from the liquid fraction measured by the lowest two electrodes located on the side of the column.

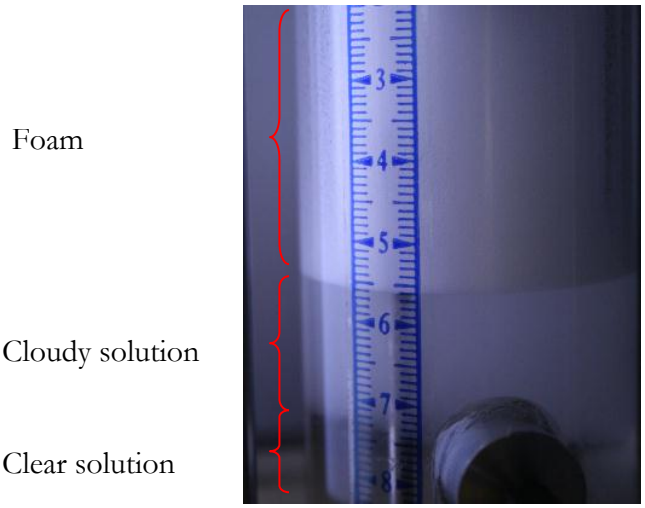

Figure 11: This figure shows the liquid-foam interface, of the Surf 4 + Surf 5 foam. The solution is cloudy, which indicated that not all the surfactant was dissolved.

The average bubble diameter was measured at a fixed height, 1000 seconds after the foaming process was concluded, see **Figure 12** for the estimations. **Figure 40** in **Appendix 1** compares the drainage rate and bubble diameter of the foam, and indicates there is a relationship between these two parameters. For more information on this relationship, see Carey and Stubenrauch [35].

The drainage rate of the foams can be influenced by the viscosity of the solution [51], and therefore the viscosity was measured of all the surfactant solutions, see **Table 5**. These viscosities of the solutions are cross-plotted against the drainage rates of the foams in **Figure 41** in **Appendix 1**. It can be concluded that the viscosities had no apparent influence on the

drainage rates of the foams.

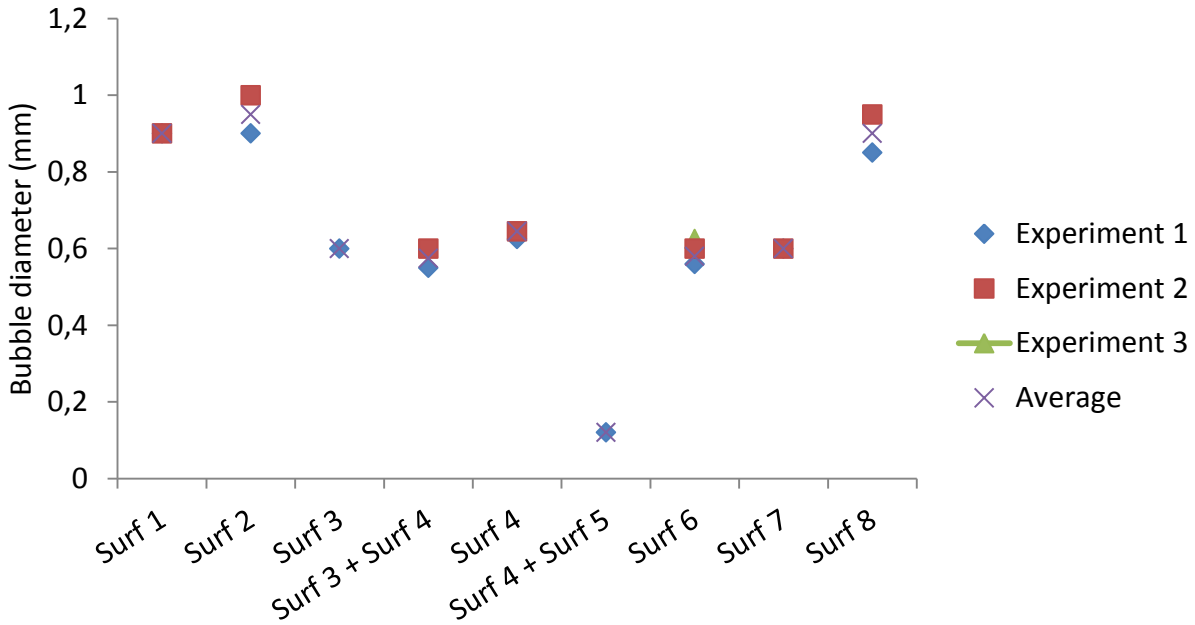

Figure 12: This figure gives the bubble diameter of the foams at a fixed height in the column, 1000 seconds after the foaming process was concluded.

Surface viscosity [mPa·s] of surfactant mixtures, determined at two shear rates [s^{-1}]		
Surfactant	Shear rate [s^{-1}]	
	2	20
Surf 1	1.22	1.08
Surf 2	1.06	1.09
Surf 3	1.12	1.08
Surf 3 + Surf 4	2.03	1.97
Surf 4	1.14	1.08
Surf 4 + Surf 5	2.31	1.45
Surf 6	1.25	1.27
Surf 7	1.11	1.07
Surf 8	1.10	1.08

Table 5: This table gives the surface viscosity of the surfactant solutions measured at a shear rate of 2 s^{-1}, and 20 s^{-1}.

2.3.2. Bulk foam in presence of oil

For every surfactant mixture, the surface tension, the interfacial tension (IFT) with hexadecane, and the pH were measured. These values are provided in **Table 6**. It can be seen that the surface tension and IFT are lower for Surf 3 + Surf 4, than for the individual surfactants. This is due to the opposite charge of the head of the different surfactant molecules, which can lead to a higher density of surfactant molecules at the interface, and thus lower surface tension and IFT [52]. Because the surfactants react in a different manner to the salt in the solution, and because the surfactants have different acid dissociation constants, the solutions differ in pH [53]. The pH does not show an obvious relationship with the half-times of the foams in absence of oil, see **Figure 9**.

Surfactant	σ(mN/m)	IFT (mN/m)	pH
Surf 1	29.139	5.067	6.39 (25.7 °C)
Surf 2	33.341	4.260	7.51 (26.1 °C)
Surf 3	29.441	2.199	7.2 (19.0 °C)
Surf 3 + Surf 4	27.517	1.543	6.82 (19.0 °C)
Surf 4	32.293	4.445	6.73 (20.4 °C)
Surf 5 + Surf 4	Not measured	4.260	Not measured
Surf 6	27.562	0.750	10.2 (21 °C)
Surf 7	28.254	4.234	6.83 (19.0 °C)
Surf 8	31.498	4.929	5.98 (22 °C)

Table 6: This table gives the surface tension (σ) of the surfactant solutions, their interfacial tension (IFT) with hexadecane, and their pH.

The reported values in **Table 6** are used to predict the stability of foam in presence of oil. The stability prediction and the half-time of the foam experiments in presence of oil are given in

Table 7 (as described in section 2.1.2). It can be seen that entering, spreading and bridging coefficients, and lamella number do not give reliable predictions on foam stability. At the end of the experiments with Surf 3, and Surf 6, we observed foam of which the liquid phase seemed more viscous than other foams in presence of oil, and were jelly-like. This was not observed with foams in absence of oil. The observed high viscosity and jelly-like appearance of foams produced with Surf 3, and Surf 6 are further discussed in section 2.3.3. The pH of the solution does not show an obvious relationship with the half-times of the foams in presence of oil, see **Table 6.**

Surfactant	$E_{o/w}$	$S_{o/w}$	Bridging	L	Half-time [s] (exp. 1)	Half-time [s] (exp. 2 dye)
Surf 1	6.769	-3.431	120	0.857	4000	2000
Surf 2	11.371	0.371	387	0.909	1000	1000
Surf 3	4.171	-0.229	117	2.007	26000	27000
Surf 3 + Surf 4	1.145	-1.855	-17.1277	2.712	80000	26500
Surf 4	5.284	-3.716	64	0.942	8500	6600
Surf 5 + Surf 4					2300	3300
Surf 6	0.892	-0.708	6	5.168	22000	23000
Surf 7	9.123	0.523	307	1.127	3700	3800
Surf 8	8.928	-0.872	262	0.964	1400	2000

Table 7: This table gives the entering, spreading, and bridging coefficient for the different surfactants, and their lamellae number, and half-times. For the lamellae number, r_o/r_p was taken to be 0.15 [42]. The surface tension of hexadecane was taken to be 27.47 mN/m [46]. A red colored cell indicates that, according to the appropriate theory, the foam is predicted to be unstable with hexadecane, yellow indicates that the foam is predicted to be moderately stable, and green indicates that the foam is predicted to be stable [42, 43, 54, 55]. The same color coding is used for the half-time to indicate what we considered stable, moderately stable, and unstable.

The average drainage rate [-] was calculated for the foams which did not collapse immediately after the foaming process was concluded. The drainage rate cannot be calculated during collapse, see section 2.1.1.1. **Figure 13** gives the drainage rate of foam in presence of oil, and in absence of oil. It can be seen that the drainage rates of the foams in presence of oil can be different from the drainage rate of foams in absence of oil. In Stubendrauch and Carey [35] a drainage rate between 2/3 and 1 indicates a Poiseuille flow regime, and between 1 and 2 a plug-like flow regime, the drainage rate of Surf 6, averaged over the two experiments, was 0.34.

Similar to the experiments of foam in absence of oil, the bubble diameter was measured of the foam in presence of oil, 1000 seconds after the foaming process was concluded, see **Figure 14**. The bubble diameters are smaller than for foam in absence of oil, which can be caused by the difference in the foaming process. A comparison of the drainage rates and the bubble diameters of the foams in presence of oil, shows that unlike foam in absence of oil, these two parameters do not show an obvious relationship for foam in presence of oil, see **Figure 42** in **Appendix 1**.

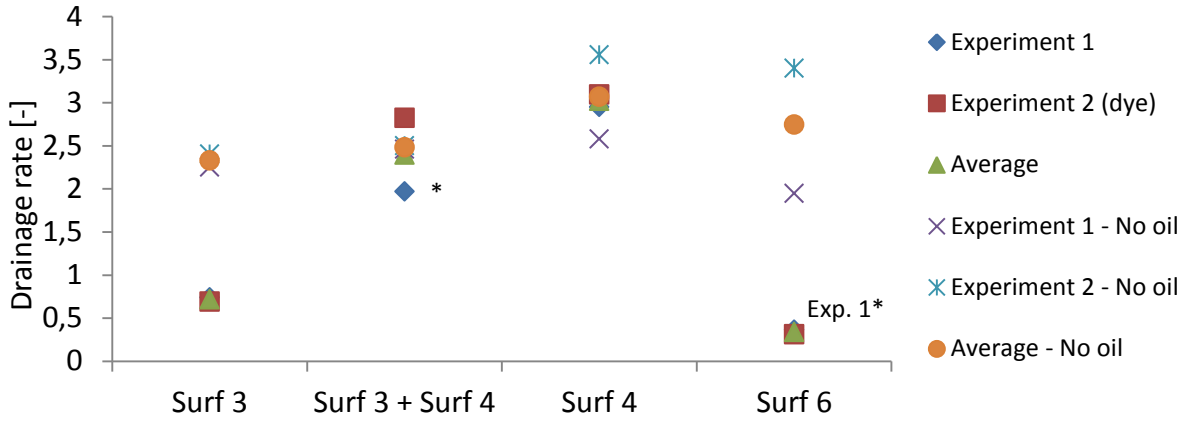

Figure 13: This figure gives the drainage rate of the foams in presence of oil, and in absence of oil. *: The liquid weight was not measured after the experiment, and we used the average value of 100.5 grams.

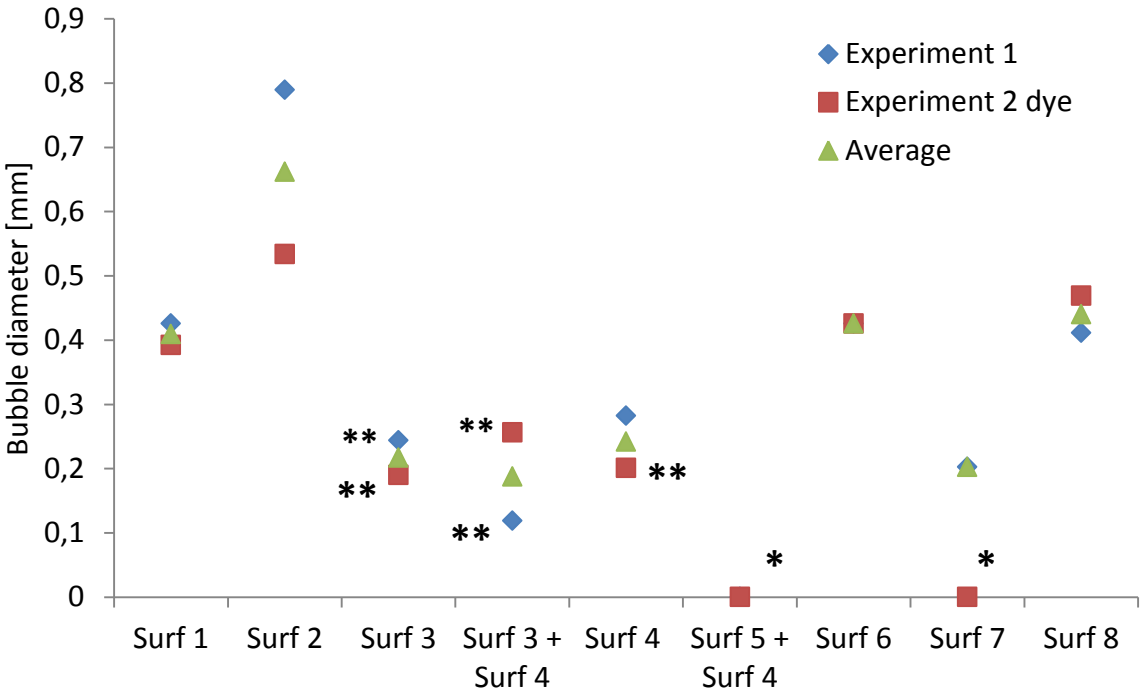

Figure 14: This figure shows the bubble diameter [mm] of the foams in presence of oil. The measurements were performed 1000 s after the foaming process was concluded. The measurements were made at the same height of the column. *: The bubbles were too small to distinguish in the picture. **: Bubbles were difficult to distinguish due to their size; therefore the size of a big bubble was determined by counting pixels, and thus the average bubble is smaller.

In the experiments of foam in presence of oil, the foam was produced by stirring the mixture with an immersion mixer for 30 seconds, and unlike the experiments of foam in absence of foam, the initial foam volume is not fixed. **Figure 15** shows the foam volume after the foaming process. Surfactants, which produced foam with a high initial volume, are considered to have a good foamability. Surfactants, which produced foam with a low initial volume, are considered to have a poor foamability, e.g. Surf 6. **Figure 43** and **Figure 44** in **Appendix 1** show cross-plots of the initial foam volumes and the drainage rates, and with the half-times of the foams. These cross-plots do not show an obvious relationship between the initial foam volume and drainage rate, or with half-time of the foams.

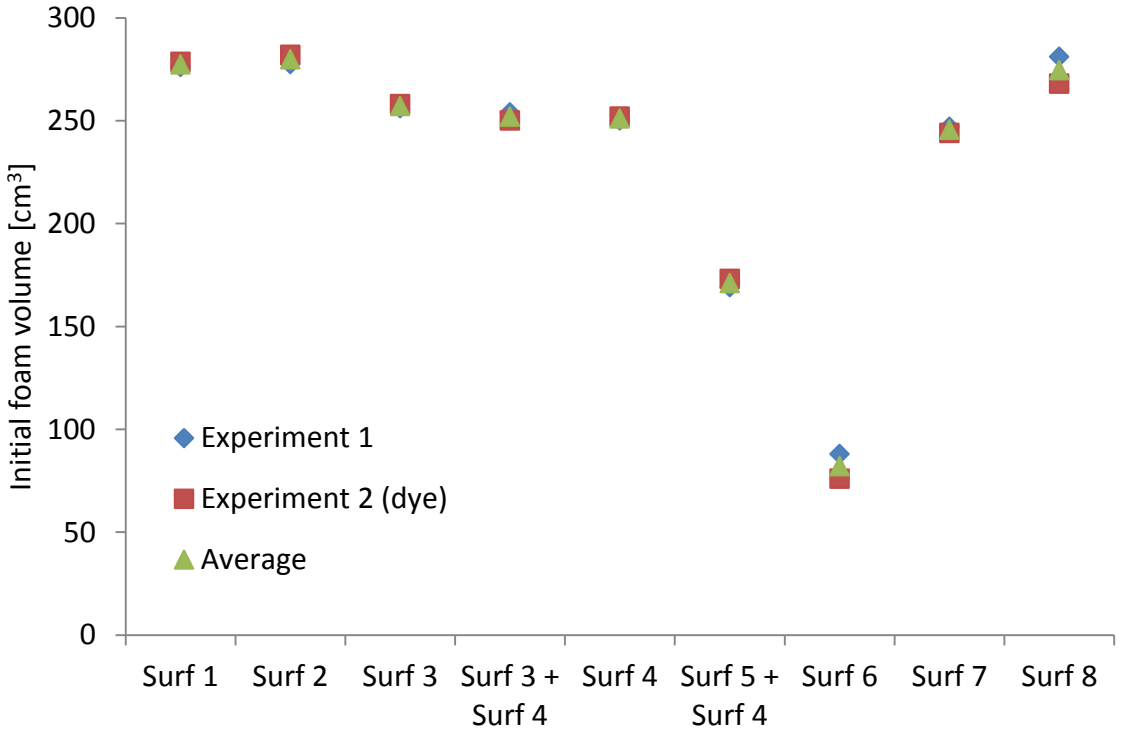

Figure 15: The figure shows the initial foam volume of the different surfactant solutions for the experiments in presence of oil.

For the experiments of foam in presence of oil, an emulsion would form under the foam column, see **Figure 16**. The typical development of an emulsion volume is shown in **Figure 17**. The maximum emulsion volume of every experiment is given in **Figure 18**. The emulsion volume was reflected in the color of the foam in presence of dyed oil. Foams with a small emulsion volume had a deeper red color, compared to foams with a large emulsion volume. **Figure 45** and **Figure 46** in **Appendix 1** show cross-plots of the maximum emulsion volumes and half-times of the foams, and with the drainage rate. These figures do not show an obvious relationship of the maximum emulsion volume with the foam stability, or drainage rate.

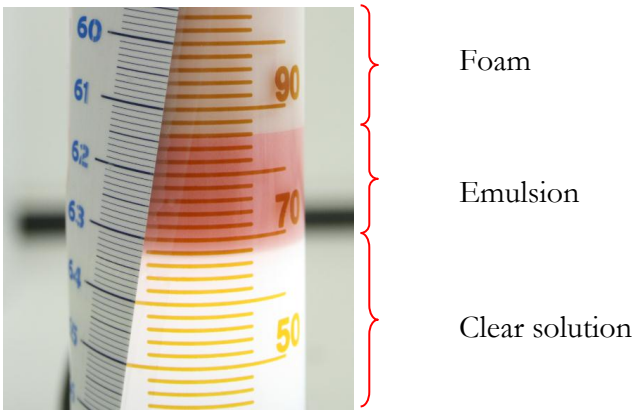

Figure 16: This is a snapshot of an experiment of foam in presence of dyed oil. The water phase is visible at the bottom of the picture, at the top of the picture the foam is visible, and in the middle an emulsion is visible.

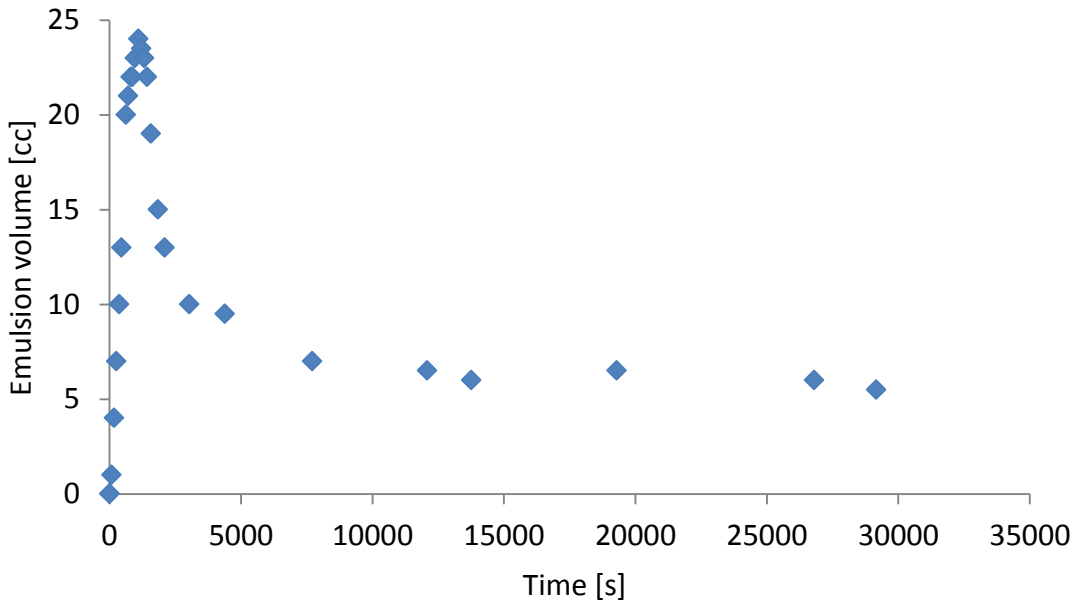

Figure 17: This figure shows the emulsion volume development of the foam experiment of Surf 3 + Surf 4 + dyed oil.

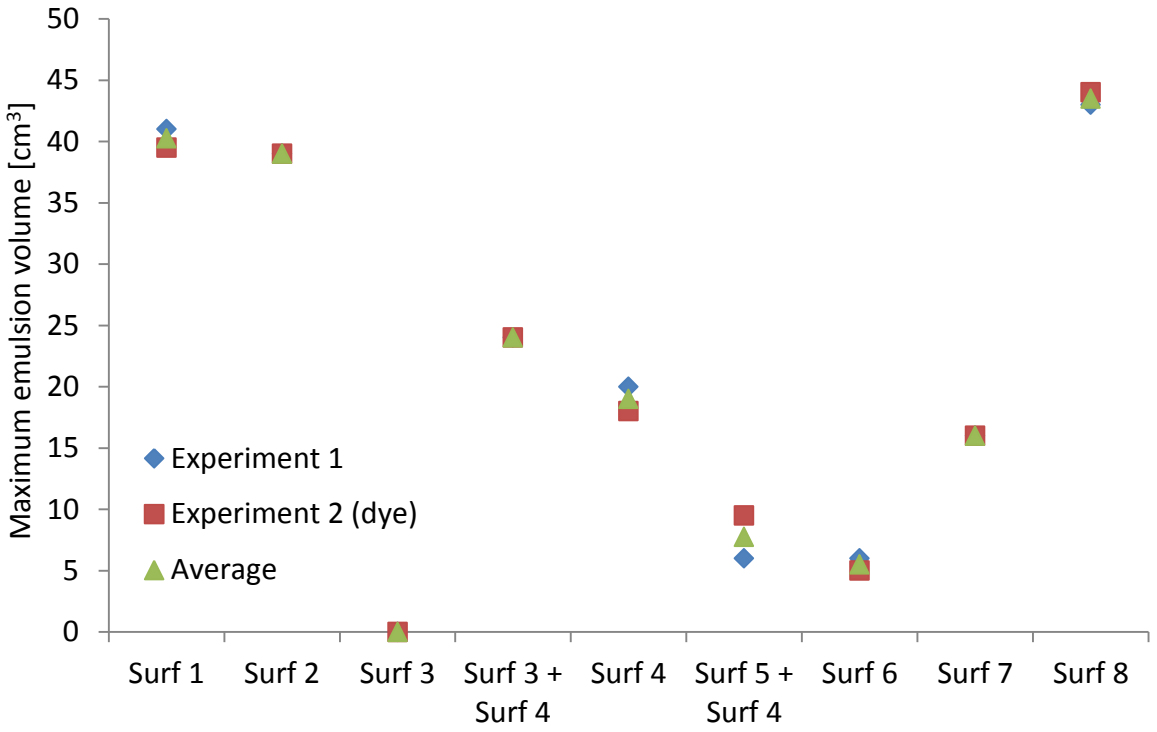

Figure 18: An emulsion forms under the foam column in the experiments of foam in presence of oil. This figure shows the maximum emulsion volume for the different surfactant solutions.

2.3.3. Discussion on experimental results

2.3.3.1. Discussion on foams in absence of oil

For only three solutions the half-times of both experiments of the foams were recorded as less than 10000 seconds, namely: Surf 2, Surf 6, and Surf 8, see **Figure 9**. The foams of Surf 2, and Surf 8 had relatively large bubble diameters at 1000 seconds, and Surf 6 had average sized bubbles at 1000 seconds, see **Figure 12**. The drainage rate of foams of Surf 2, and Surf 6 were average, and for Surf 8 the drainage rate was above average, see **Figure 10**. Therefore it can be said for the foam of Surf 6 that the film thickness development over time was similar to that of more stable foams. Since the half-time is relatively short, it can be said that the critical capillary pressure of the foam of Surf 6 is lower than for more stable foams, see **Figure 3** and section 2.1. The bubbles of Surf 2 grew larger relatively fast, and thus the gas diffusivity is higher than in other solutions. This leads to thinner films in the foam of Surf 2 compared to more stable foams, and this partly explains why Surf 2 had a relatively short half-time; a relatively low critical capillary pressure can also be a factor. The bubbles of the foam of Surf 8 grew relatively fast, and the drainage rate was relatively high. Even though the foam of Surf 8 might have a similar critical capillary pressure as the more stable foams, its other characteristics lead to a shorter half-time.

The experiments with Surf 1, Surf 3, Surf 3 + Surf 4, Surf 4, Surf 4 + Surf 5, and Surf 7 were all stopped before half-time was reached, see **Figure 9**, and were considered relatively stable foams. As mentioned in section 2.3.1 not all the surfactant was dissolved in the mixture of Surf 4 + Surf 5, see **Figure 11**. Therefore the behavior of the foam cannot be assumed to be similar to that of the other foams, which were made out of homogenous solutions. It was observed that drainage rate was lower than, and the average bubble size, 1000 seconds after foaming, was smaller than the other stable foams, see **Figure 10** and **Figure 12**. This could have been caused by the floating particles in the surfactant mixture.

2.3.3.2. Discussion on foams in presence of oil

The theory of the lamella number (which should predict the foam stability in presence of oil) was proposed by Schramm and Novosad [42, 43]. The proposition was based on results of experiments in which they let a "train" of foam bubbles move through a horizontal capillary, see **Figure 19**. An oil droplet was located at the side of the capillary and it was monitored if the oil droplet would enter the "train" of foam bubbles from the side of the capillary and if it would make the bubbles collapse. It was in these experiments that the droplet size ratio in the *lamella number* (r_o/r_p) was found to be 0.15. Because the foam was not placed in a vertical capillary, drainage did not play a role in their experiments.

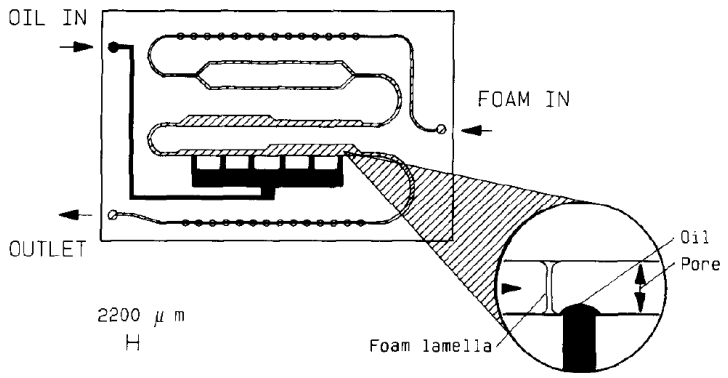

Figure 19: Micro-visual cell plate showing the etched flow pattern, approximately to scale, and the arrangement of phases at initial contact, adapted from Schramm and Novosad [42].

Unlike in Schramm and Novosad [42], we forced oil to be mixed with foam by stirring the surfactant-oil mixture in our experiments. Because we use the immersion mixer, the oil consists of small droplets in the foam, initially. Therefore the experiments that were performed in this research are significantly different from the experiments performed by Schramm and Novosad [42]. Most likely r_o/r_p cannot be considered to be equal to 0.15 in our research. Moreover, because drainage did not take place in Schramm and Novosad [42], but took place in our research, and due to the other apparent differences, the lamella number theory cannot be assumed to hold in our research.

The foams of Surf 3, and Surf 6 had low drainage rates, relatively small emulsion volumes, were stable, and were observed to have high viscosities and seemed gel-like, see **Figure 13**, **Figure 18**, and **Table 7**. Microemulsions of oil, water and surfactant reportedly can be viscous and gel-like, both in water-rich as well as in oil-rich mixtures [56, 57]. Chen et al. [56] report that a microemulsion of 32 wt% water, 51 wt% tetradecane, and 17 wt% surfactant has a viscosity of 44 mPa·S. A gel-like behavior of the foams formed with Surf 3 and Surf 6 partly explains the low drainage rate, and high stabilities. However, this does not explain why for the foams of Surf 3 the oil did not drain out of the foams but the solution did, similarly for Surf 6 the oil drained out of the foams at a lower rate than the solution.

Unlike for foam in absence of oil, the drainage rate of foam in presence of oil is not correlated to the bubble diameter, see **Figure 40** and **Figure 42** in **Appendix 1**. This can be explained by the change in viscosity and gel-like behavior.

We propose the following explanation for the observed half-times

If the IFT between the hexadecane and the surfactant is relatively high, the oil will form relatively big droplets over time [58]. As the foam becomes drier, the lamellae become thinner, and foam becomes more fragile. Due to Ostwald ripening of the oil droplets, the average oil droplet becomes bigger over time [58, 59], and will break the foam because of the limited elasticity of the Plateau borders. Thus, this process is not related to the entering, spreading, or bridging coefficient, but is rather a steric effect.

If the IFT is low, the oil droplets will grow at a lower rate than at a higher IFT [58], and will be completely covered by surfactant molecules, and due to the low IFT and small size, have little impact on the foam stability. It was observed that the liquid phase of the foams produced with Surf 3, and Surf 6 were relatively viscous and were gel-like. This can explain the relatively low drainage rates, and high stability of these foams, see **Figure 13** and **Table 7**. The foams of Surf 3 + Surf 4, and Surf 4 did not seem gel-like, nor did it seem that they had undergone any changes in viscosity, which can explain why the drainage rates were unaffected by oil. **Figure 20** gives a scheme, which summarizes our explanation of our observations of the behavior of foam in presence of oil in our experiments.

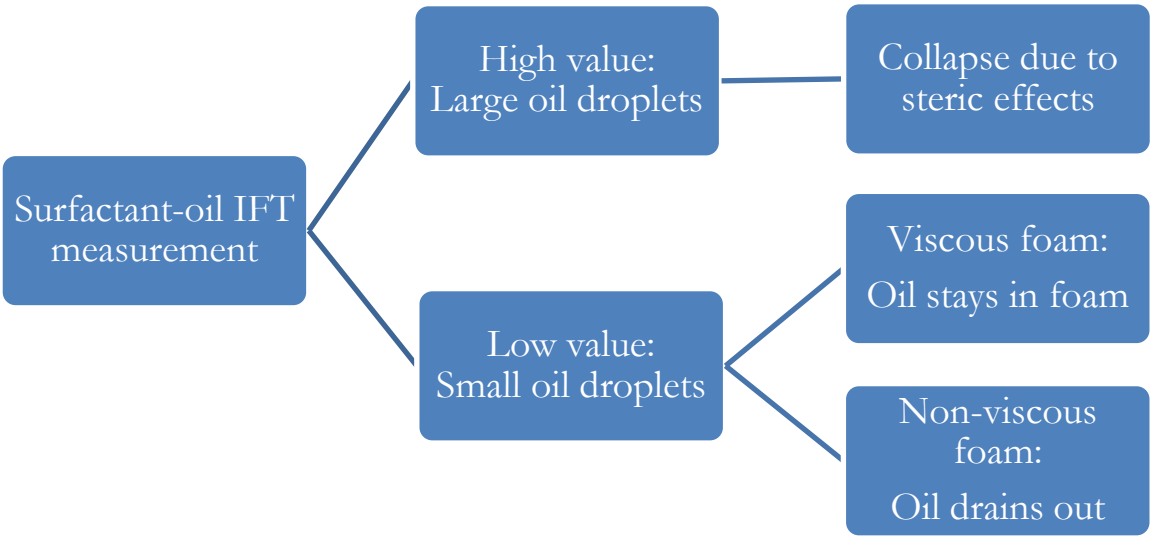

Figure 20: This scheme gives our theory for our observed behavior of foam in presence of oil.

2.4. Conclusions and recommendations

2.4.1. Conclusions

- The FoamScan foam volume measurements can be unreliable at a low liquid fraction of the foam.
- Properties of bulk foam in absence of oil do not give a reliable prediction on the behavior of bulk foam in presence of hexadecane.
- Unlike foam in absence of oil, the average bubble diameter of foam in presence of oil (at 1000 seconds after the foaming process) does not correlate with the drainage rate. This can be due to the change in viscosity and gel-like behavior of the liquid phase in the foam.
- Surf 3, and Surf 6 produce foams with a lower drainage rate in presence of oil, than in absence of oil. Visually, the liquid phase of the foams appears to be more viscous than for the same foams in absence of oil, which could be the reason for the change in drainage rate.
- An emulsion forms under the foam column in experiments of foam in presence of hexadecane. The emulsion volumes do not show an obvious correlation with other investigated parameters of the surfactants and oil.
- The combination of the entering, spreading, and bridging coefficient did not give a reliable prediction on the behavior of foam in presence of hexadecane in this research.
- Contrary to the suggestions in Schramm and Novosad [42], the unstable foams in this research had lamella numbers lower than stable foams.
- A mixture of a surfactant that forms unstable foam in presence of hexadecane, and a surfactant that forms stable foam in presence of hexadecane, can form foam which is more stable in presence of hexadecane than the individual surfactants.

2.4.2. Suggestions for future research

- The volume measurements by the FoamScan should be verified systematically.
- Perform experiments on bulk foam in presence of oil, by foaming a mixture of Surf 3 and Surf 6, or similar surfactants, as an attempt to produce stable bulk foam in presence of oil, which has a low drainage rate, and good foamability.
- Perform experiments on bulk foam in presence of oil to add more detail to the impact of surface tensions and interfacial tension on foam stability, and to investigate what influences the forming of emulsions under the foam column.
- Conceive an experimental set-up with which the viscosity of bulk foam can be measured.
- Coreflooding with foam should be performed with the same surfactant solutions. This should be done in presence of oil, and in absence of oil.

3. SAG simulations

We report a simulation study of foam injection into a water-flooded oil reservoir by a single cycle surfactant-alternating-gas (SAG). The injection pressure and production pressure were constrained. We performed several simulation runs, varying the time-period of surfactant injection, and the minimum water saturation above which foam is stable, i.e. the water saturation corresponding to the limiting capillary pressure. The time-period of gas injection was fixed. In this report we give a description of the foam front propagation, and oil production as a function of cumulative injected surfactant. We show that the effect of the foam on the cumulative oil production and cumulative gas injection is less significant if the foam loses its stability at higher water saturation.

Up to the present moment, published research on SAG does not demonstrate the impact of oil in the reservoir on the foam propagation and foam stability. We show that oil can have significant impact on foam stability and foam propagation in a reservoir, and how this can impact the flow of oil, gas, and water in a reservoir.

3.1. Introduction

We model a foam-displacement process in a 3-D porous medium. We seek the influence of the surfactant slug size, the critical water saturation for foam stability (*fmdry*), and oil in a single-cycle SAG flood on the cumulative oil production. Our model is adopted from Namdar Zanganeh and Rossen [60]. The duration of the surfactant injection is represented as *switching time* (t_s). There is neither gas nor foam in the reservoir before t_s. Gas injection starts and surfactant injection stops at t_s. The total period of injection is defined as t_s plus 250 days of gas injection. The *fmdry* is defined as a volume fraction of the fluids.

The 3D reservoir is homogeneous, box-shaped, 100mX100mX30m and modeled with 10x10x10 gridblocks, unless mentioned otherwise. The reservoir is sealed on all bounding surfaces. The reservoir has one vertical injection well and one vertical production well located at opposite corners of the reservoir, in the middle of the corner gridblocks. The wells are perforated over the entire interval and operate at a constant prescribed pressure. The reservoir simulator uses the Peaceman model [61] for injectivity into and productivity from the well gridblocks.

We investigate gas performance in sweeping oil. We simulate SAG on a water-flooded oil reservoir. Therefore, we set the initial oil saturation in the reservoir at the residual oil saturation to water flood (S_{orw}). We assume that the injected surfactant does not affect the interfacial tension between the oil phase and the aqueous phase. Since the level of surfactant adsorption does not fundamentally alter the foam-displacement process, it is excluded in this study for simplicity. The three liquid phases are assumed to be completely immiscible. Due to these assumptions and simplifications the oil is neither displaced nor produced before the switching time. We set the residual oil saturation to gas flood (S_{org}) lower than S_{orw}, and thus, though the injected gas is defined to be immiscible with the oil, the gas is capable of displacing the remaining oil.

The three-phase permeabilities are calculated by equations in **Appendix 2**. The values of parameters for the relative-permeability model and the foam model are summarized in **Table 8**. Foam is modeled as gas of which the mobility is reduced, and thus this model is a three-phase model. To calculate the three-phase relative permeability we use saturation weighted model, see Baker [62].

We summarized the reservoir and fluid properties in **Table 9** and **Table 10.** There is no gas in the reservoir initially, the initial oil saturation is 0.3 (=S_{orw}), and the initial water saturation is 0.7. The surfactant concentration of the surfactant slug is 0.24 wt%, which is well above the minimum concentration required for foaming in the model. The water phase and oil phase are incompressible, and the gas phase is slightly compressible in the simulations (i.e., c_g = 1.68E-8 Pa^{-1}). We summarized the assumptions in the work in **Table 11**.

Parameters	Values
epdry	1000
epcap	1
epoil	1.5
epsurf	1
floil	0
fmdry (S_w*)	0.2/0.316
fmmob	1000
fmoil (S_o*)	0.4
fmsurf (C_s*)	0.0012
k_{rg}^0	0.94
k_{rog}^0	0.8
k_{row}^0	0.8
k_{rw}	0.3
n_g	3
n_{og}	3
n_{ow}	2
n_w	4
S_{gr}	0
S_{org}	0
S_{orw}	0.3
S_{wir}	0.1
S_{wi}	0.7

Table 8: Parameters of the relative permeability model and foam model (Namdar Zanganeh and Rossen [60]).

Parameters	Values
Length (m)	100
Width (m)	100
Height (m)	30
Depth (m)	1600
Δx (m)	10
Δy (m)	10
Δz (m)	3
ϕ	0.2
k_x (mD)	100
k_y (mD)	100
k_z (mD)	10
$C_{s,inj} = 2C_s$*	0.0024
P_{ref} (bar)	165
P_{wf}^{inj} (bar)	250
P_{wf}^{prod} (bar)	145
*2.4 g of surfactant in 1 kg of surfactant solution	

Table 9: Reservoir properties, simulation parameters, and well constraints (Namdar Zanganeh and Rossen [60]).

Parameters	Values
μ_g (cp)	0.02
μ_o (cp)	5
μ_w (cp)	0.47
ρ_g (kg/m^3)	306.6
ρ_o (kg/m^3)	900
ρ_w (kg/m^3)	985
c_g (Pa^{-1})	1.68 x 10^{-8}
c_o (Pa^{-1})	0
c_w (Pa^{-1})	0

Table 10: Fluid properties at reservoir conditions (160 Bar, 60 °C) (Namdar Zanganeh and Rossen [60]).

- Reservoir is rectangular and homogeneous (constant porosity and permeability), and heterogeneity is disregarded.
- Surfactant adsorption on the rock is ignored.
- Surfactant is only soluble in the water phase.
- Miscibility is not allowed between phases.
- Initially there is no gas present in the reservoir.
- Initial oil saturation in the reservoir before surfactant injection is at $S_{orw} = 0.3$.
- There is no reduction in S_{orw} with the introduction of surfactant into the aqueous phase.
- Gas, though immiscible, is capable of displacing oil; we set the S_{org} lower than S_{orw}.
- The gas phase is slight compressible, and other phases are incompressible in the simulations.

Table 11: Simulation assumptions (Namdar Zanganeh and Rossen [60]).

Our foam model takes into account the effects of water saturation, oil saturation, and surfactant concentration in the aqueous phase on the foam strength. The gas relative mobility of the gas phase in the absence of foam (λ_{rg}^{nf}) is scaled by a function, *MRF*, to take into account the effect of lamellae on gas mobility, while the liquid mobilities remain unchanged. *Fmmob*, in **Eq. (13)** is the maximum reduction of the gas mobility, in the absence of factors that increase the average bubble size [63]. F_w, F_o, and F_s describe the stability of foam as a function of water, and oil saturation and surfactant concentration respectively; they are defined in **Appendix 4**.

In our foam model, low water saturation can weaken foam, according to **Eq. (21)**. Next to that, oil saturation above a certain threshold value kills foam, according to **Eq. (22)**. F_s reaches its maximum above a certain surfactant concentration, C_s^* (0.12 wt% in our simulations); the exact relation of foam to the surfactant saturation is given in **Eq. (23)**. In this foam model, a small change in water saturation can cause an abrupt change in foam strength, which is in agreement with laboratory data [64, 65]; this is further discussed in **Appendix 4**.

This research is performed as a case study to shed light on the competing goals behind foam processes, and does not describe any particular field application.

$$\lambda_{rg}^{f} = \frac{\lambda_{rg}^{nf}}{MRF}, \qquad where\ MRF = 1 + fmmob\ \times F_w\ \times F_o\ \times F_s \qquad \textbf{(13)}$$

3.2. Simulation results and discussions

3.2.1. Varying the switching time

We performed single cycle SAG simulations at various surfactant injection times, which we call switching times here, and fixed gas injection time (250 days). The injection, and production well were set at fixed pressures. The pressure difference of the injection well with the reservoir determined the surfactant injection rate, and later on the gas injection rate. The surfactant injection rate was constant, which can be seen in **Figure 21**.

Independent simulations were run with various switching times, and the cumulative produced oil and cumulative injected gas were recorded at the end of the simulations. We ran these single cycle SAG simulations for two different values of *fmdry* (0.316 and 0.20), which is the water saturation below which foam is unstable. The production and injection data are plotted against the switching time in **Figure 22**. This figure shows the impact of switching time, and thus the injected surfactant-slug volume, on the cumulative oil production and cumulative gas injection. The switching time has a bigger effect for *fmdry* = 0.20 than for *fmdry* = 0.316, because the foam is generally stronger for *fmdry* = 0.20 (the strongest foam for *fmdry* = 0.20 has an apparent viscosity of about 7 cp, for *fmdry* = 0.316 it is about 0.25 cp at the end of the simulation). The reason for this will be discussed below.

Figure 23 shows the surfactant concentration in the gridblocks after two days of surfactant injection into the reservoir, and gas injection had not taken place. A yellow or green color indicates that the surfactant concentration is below the threshold value for maximum foam strength to exist. The figure shows that the surfactant is mainly located in the gridblocks surrounding the injection well, and foam will form in these gridblocks when gas is injected. The injected gas will turn into foam in these gridblocks, affecting the permeability of these gridblocks somewhat similar to a skin. The Injectivity Index has a logarithmic relationship with the radius of the skin. Therefore, in the gridblocks surrounding the injection well, the foam has a relatively strong affect on the cumulative gas injection, and thereby the cumulative oil production, see **Figure 22**. **Figure 24** shows that the oil bank ahead of the foam front did not reach the production well at the end of the simulation.

If surfactant is injected for 18 days or less, less oil is produced compared to the gas flooding case, because less gas is injected. This can be seen in **Figure 25**, which shows the ratio of cumulative gas injected to oil produced (Gas Utilization Factor, or GUF), and each point represents the ratio recorded at the end of an independent simulation.

As more surfactant is injected, more foam will be able to form, and thus the foam-front will be closer to the production well at the end of the simulation. Ahead of the foam-front there is an oil bank, which reaches the production well if surfactant is injected for at least 18 days, see **Figure 26**, and thus if surfactant is injected for more than 18 days, the GUF is less than for gas flooding, see **Figure 25**.

The maximum foam viscosity can be achieved when the surfactant concentration in the water is higher than *fmsurf*, which is 0.12 wt% in our simulations. Hence, when all gridblocks through which the gas travels have at least this surfactant saturation, the minimum GUF and the maximum cumulative oil production are reached. This is the case for switching time = 61 days, see **Figure 27** and **Figure 28**. After gas injection the surfactant is more spread out over the reservoir compared to before gas injection, as can be seen in **Figure 29** and **Figure 27**. Therefore foam can form in more gridblocks and will sweep the reservoir better than if this were not the case.

3.2.2. Impact of oil on foam front stability

We looked in detail at the SAG simulation with a switching time of 61 days and an *fmdry* of 0.20, to investigate the impact of oil on the foam-front stability. We saw that at the end of the simulation foam was not present in every gridblock, see **Figure 30**, even though the surfactant concentration in the water was higher than *fmsurf* in most of these gridblocks, see **Figure 27**. **Figure 31** shows the water saturation in the gridblocks at the end of the simulation, and it can be seen that the water saturation at top of the reservoir is below 0.20, which is the threshold value below which foam is weaker. *fmoil* is the threshold value above which foam cannot exist, and it is set to 0.40 in these simulations. **Figure 33** shows the oil saturation in the gridblocks at the end of the simulation. It can be seen that the oil saturation is higher than 0.40 at the bottom of the reservoir. Therefore gas overrides the foam at the top of the reservoir, and foam overrides the oil at the bottom of the reservoir. These differences in phase saturation are present because foam collapses at high oil saturations, and the liberated gas moves up in the reservoir because it is relatively light, and it pushes down water and oil in this process. Eventually the water saturation will be too low for stable foam to exist at the top of the reservoir, and similarly the oil saturation will be too high at the bottom of the reservoir. Therefore, the phenomenon, which is visible in **Figure 30**, is not overriding in the classical sense, which is solely caused by density differences. This theory is supported by the results of a similar simulation in a 2D reservoir, which has dimensions 1mX100mX30m (modeled with 1x10x10 gridblocks). This is illustrated in **Figure 36**, **Figure 37**, **Figure 38**, and **Figure 39**, which show the oil, and water saturation, and the gas viscosity in the gridblocks, and the volume fluxes of the phases at the end of the simulation.

The effect of foam on oil is less obvious for the case of *fmdry* = 0.316 and switching time equal to 61 days. Because the water saturation is below *fmdry* in more gridblocks for *fmdry* = 0.316, compared to the case of *fmdry* = 0.20, foam is less strong than for the case of *fmdry* = 0.20, see **Figure 31** and **Figure 32**. This is reflected in the lower cumulative oil production and gas viscosity at the end of the simulation for *fmdry* = 0.316, compared to *fmdry* = 0.20, see **Figure 22**, **Figure 30**, and **Figure 34**. Weak foam will form a less significant oil bank in front of it, and thereby oil is more homogeneously distributed over the reservoir, see **Figure 35**, than for relatively strong foam, see **Figure 33**.

Figure 24, **Figure 26**, and **Figure 33** show the oil saturation at the end of the simulations. The oil saturation changes abruptly over some gridblocks at the bottom of the reservoir. This could be caused by errors in the simulator, or by physical phenomena, which are not well captured in a course grid, as in the simulations of this research.

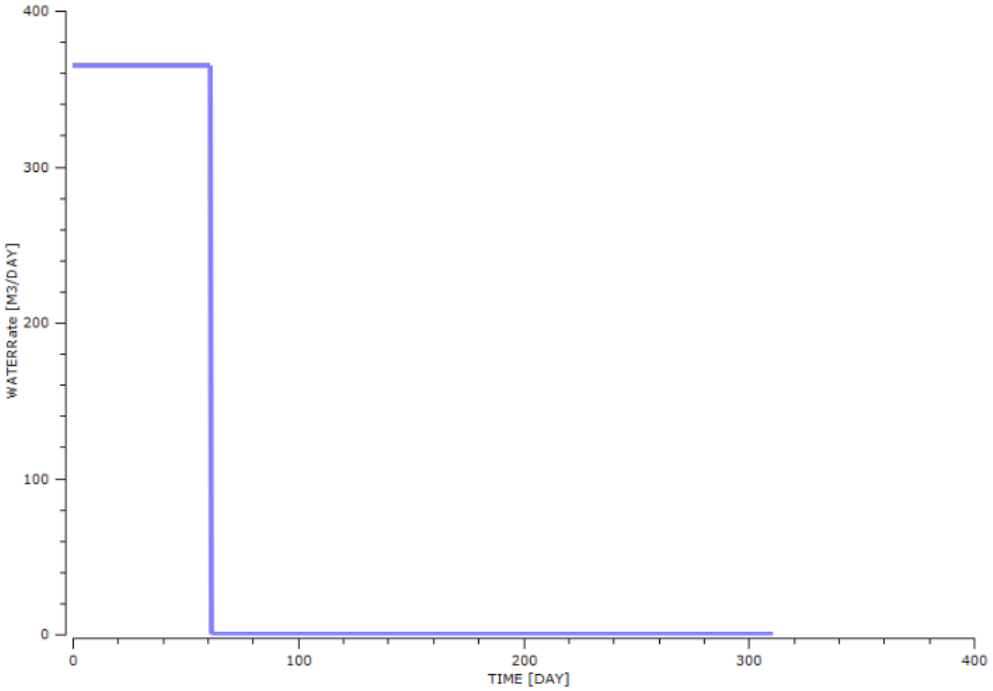

Figure 21: Surfactant injection rate for a switching time = 61 days, and *fmdry* = 0.20.

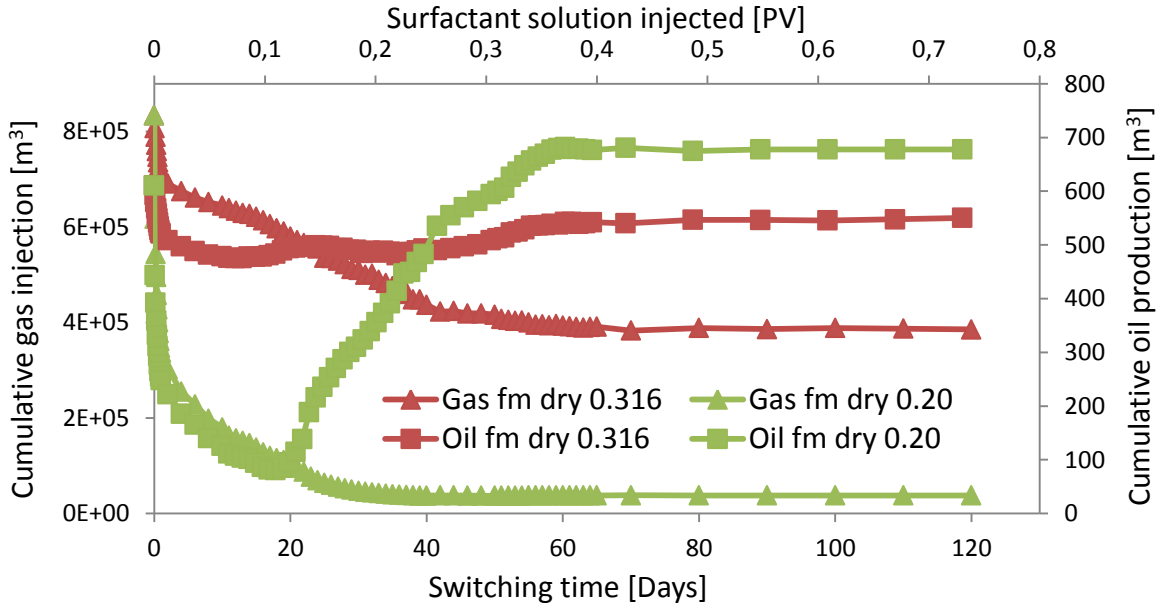

Figure 22: Cumulative oil produced and cumulative gas injected vs. switching time [in days and in pore volumes (PV)] for the two different fm dry. A single, independent simulation with a certain switching time is represented by one point displaying the cumulative oil produced and one point displaying the cumulative gas produced**.**

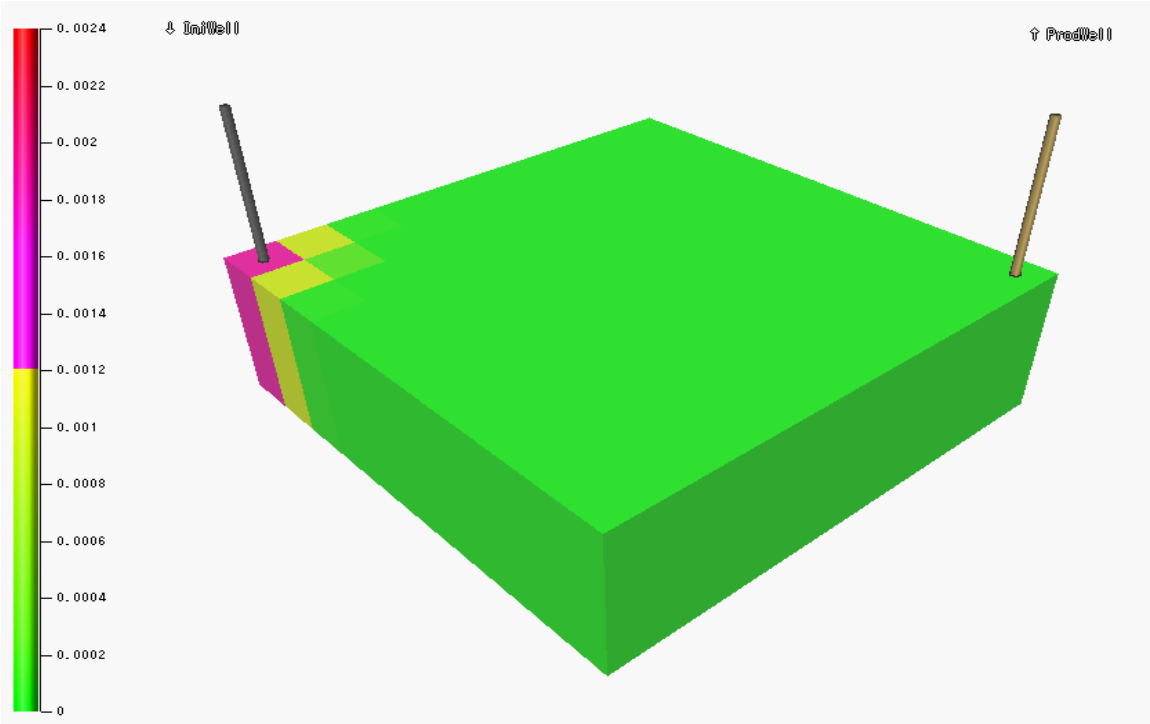

Figure 23 : The surfactant concentration before gas injection, for switching time 2 days. It is visible that the gridblocks with the well have a surfactant concentration above 0.0012, which is enough for foam to form. The surrounding gridblocks have a concentration which is below *fmsurf*.

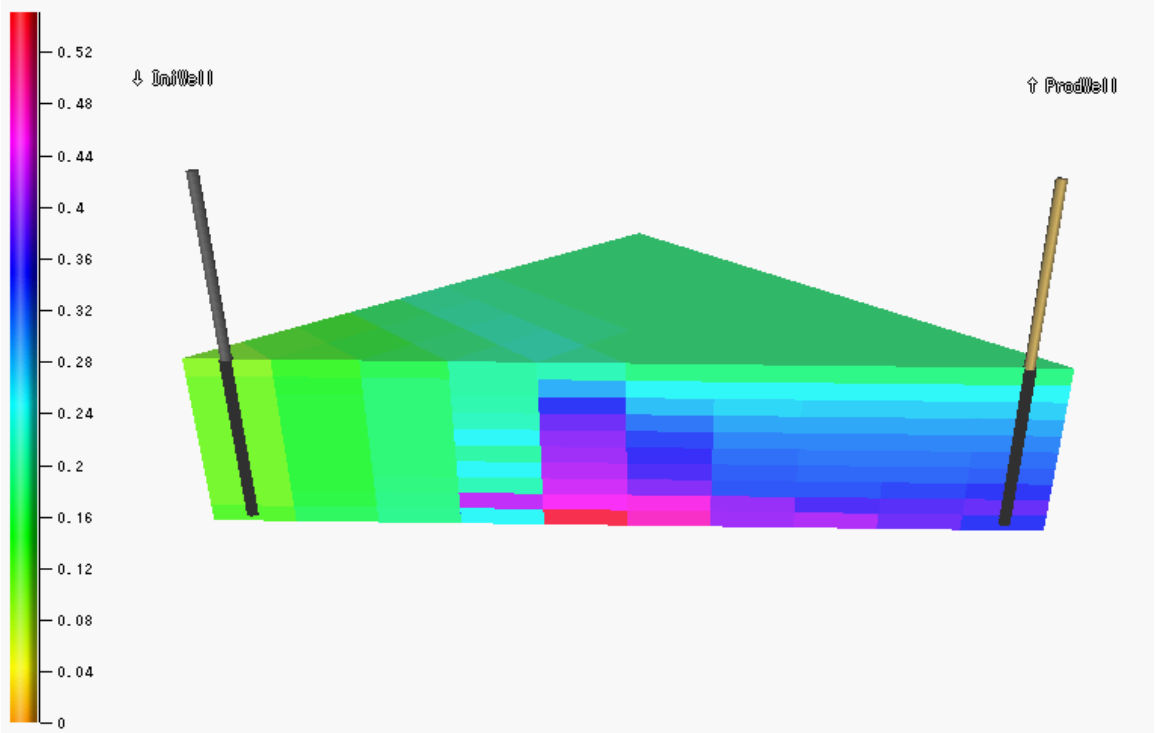

Figure 24: Oil saturation after gas injection. *Fmdry* = 0.20 and switching time is 2 days.

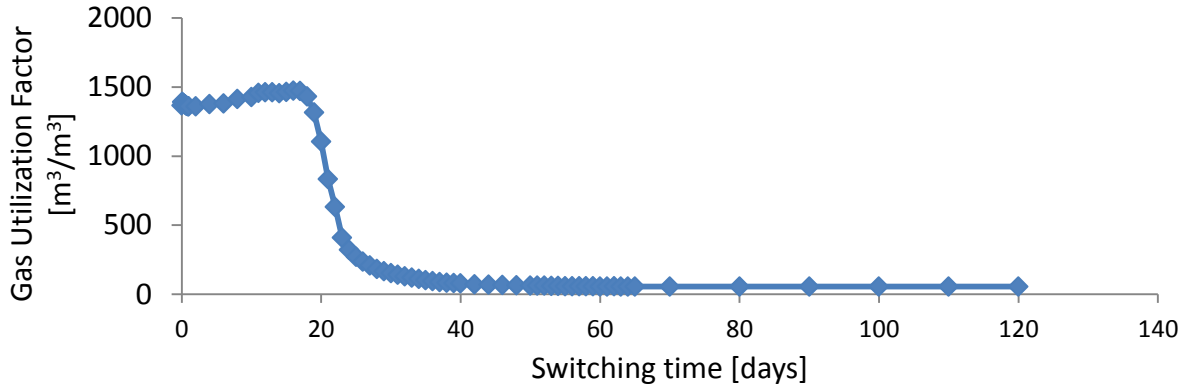

Figure 25: The gas utilization factor is the ratio of cumulative gas injected and cumulative oil produced. This figure shows the GUF for simulations run with an fm dry of 0.20.

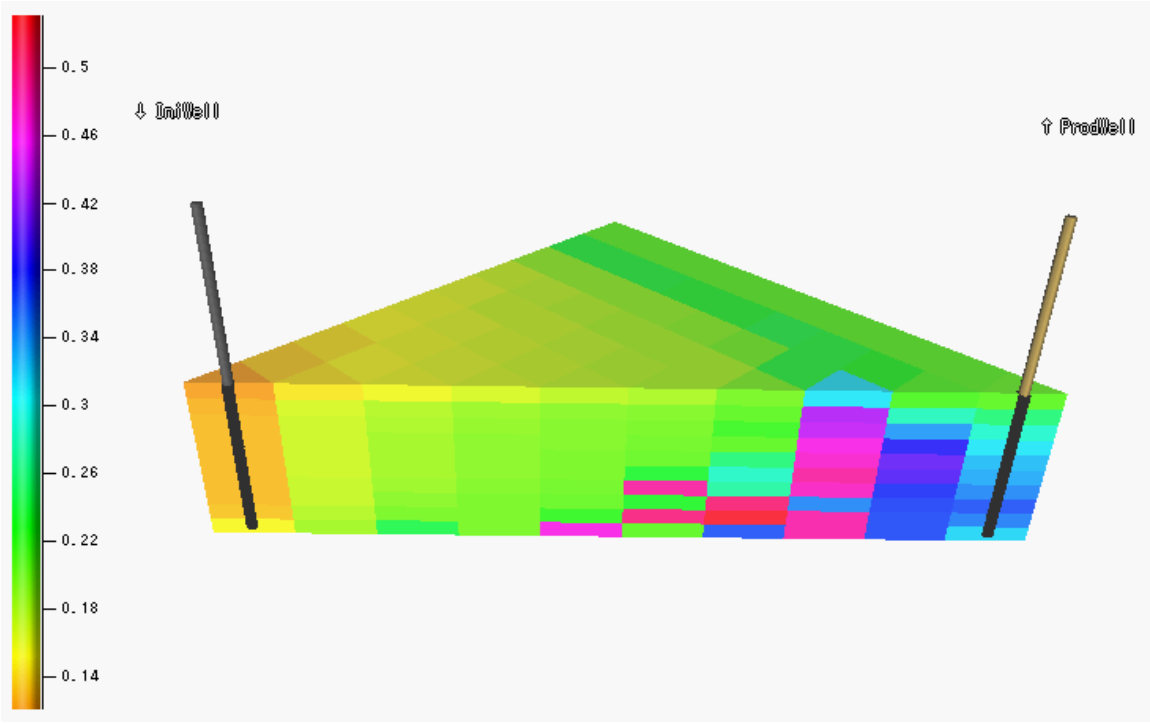

Figure 26: This figure shows the oil saturation at the end of the simulation. *Fmdry* = 0.20 and switching time = 18 days.

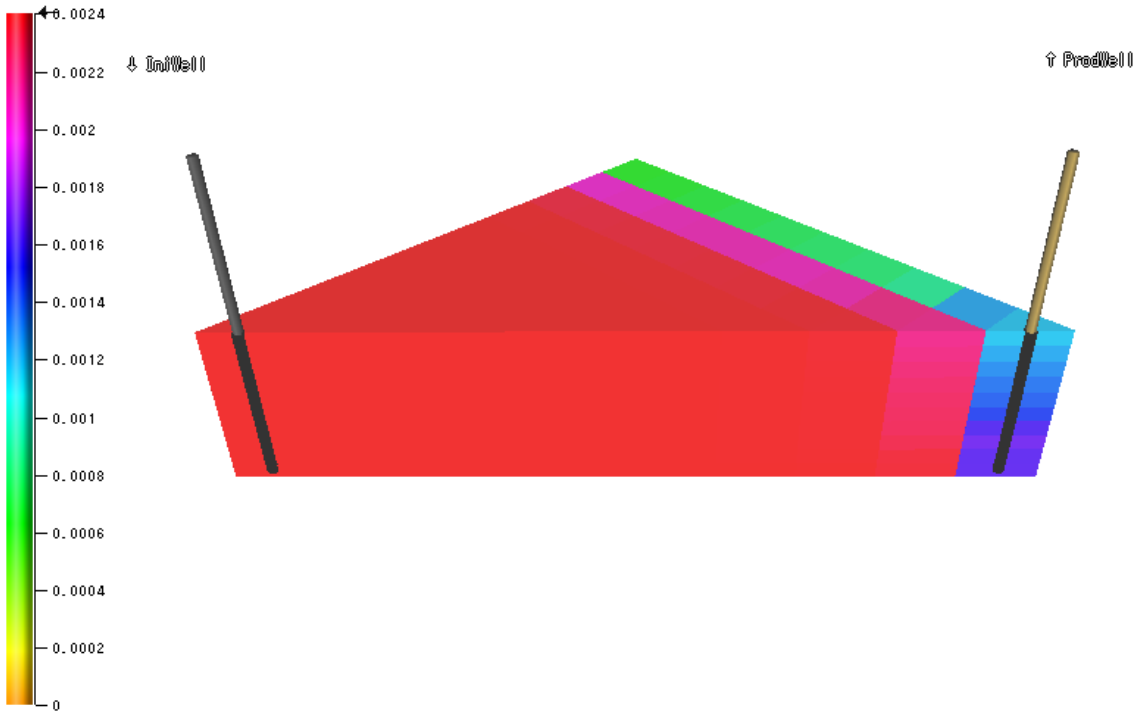

Figure 27: Surfactant concentration in the water. For *fmdry* = 0.20, switching time = 61 days, after injection gas for 250 days.

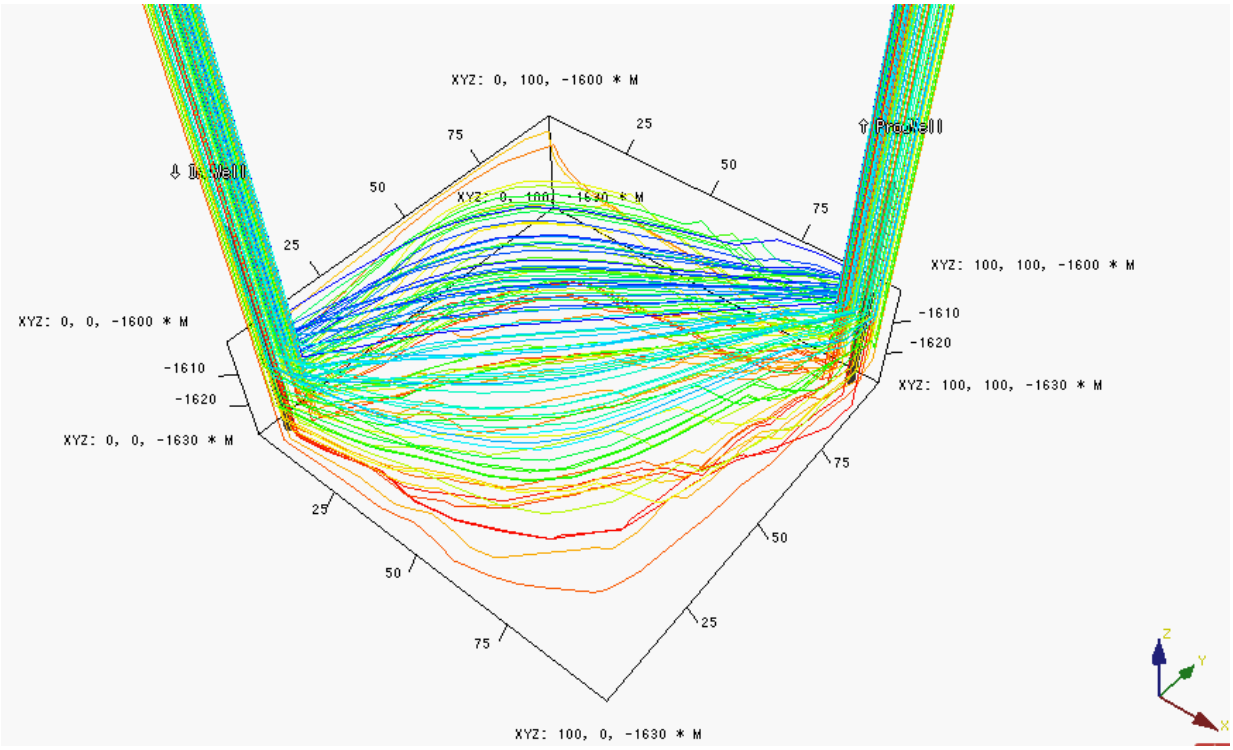

Figure 28: Display of individual gas streamlines, for *fmdry* = 0.20, switching time = 61 days at the end of the simulation.

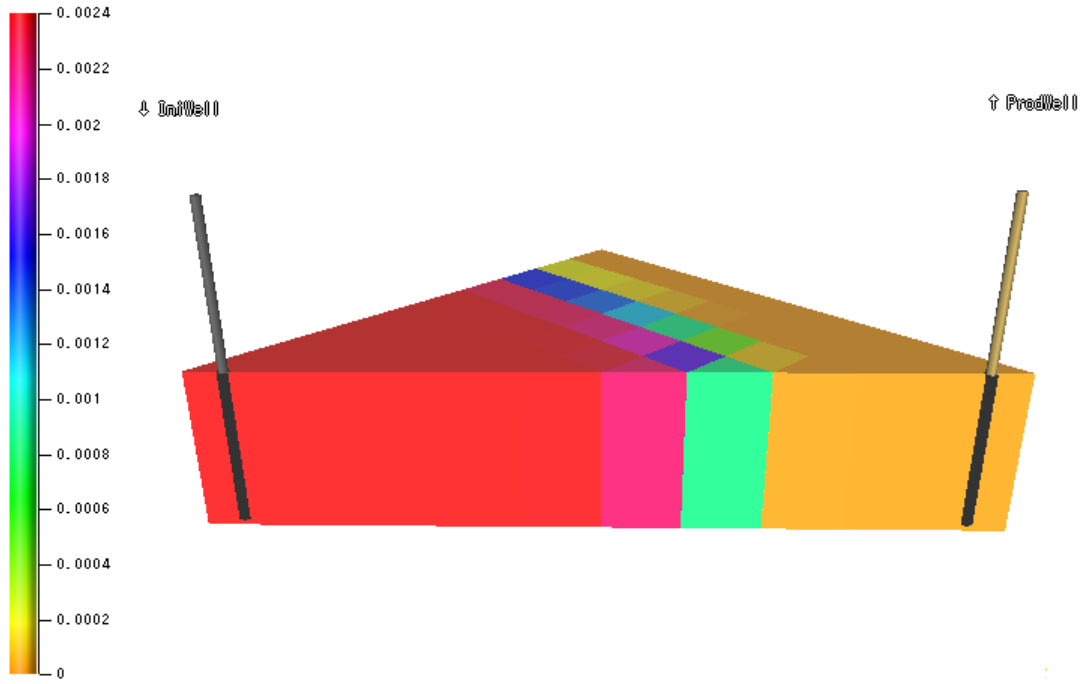

Figure 29: Surfactant concentration in the water, for a switching time of 61 days, before injecting gas.

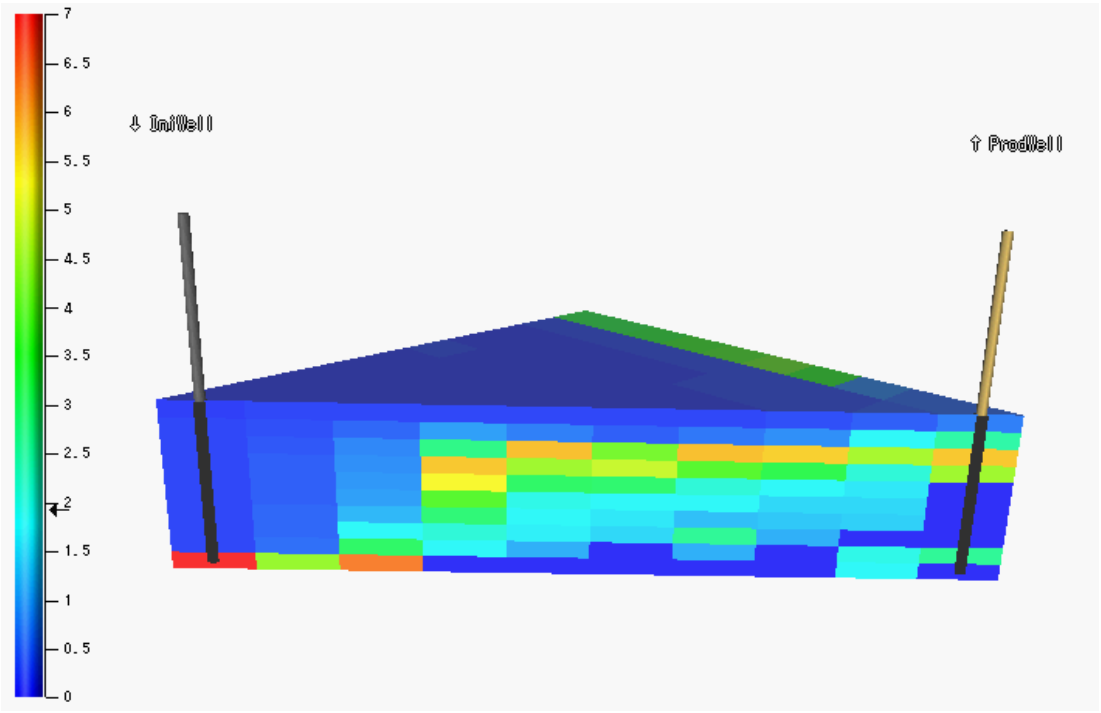

Figure 30: Gas viscosity (cP) at the end of the simulation, for fm dry = 0.20 and switching time = 61 days, and gas injection time = 250 days.

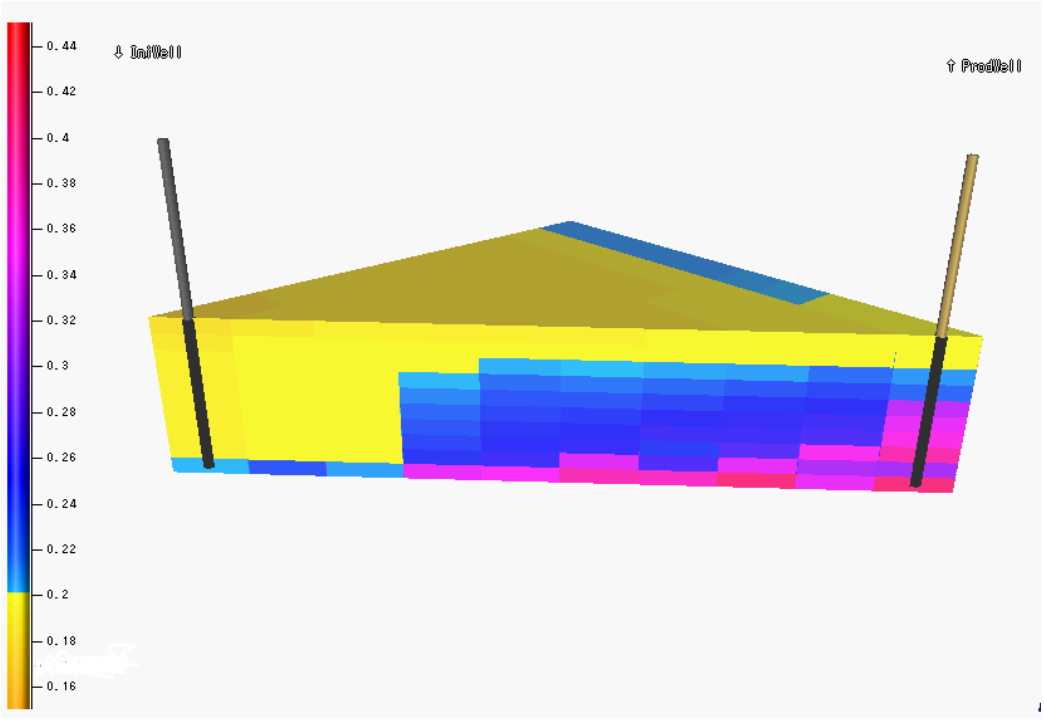

Figure 31: Water saturation in the gridblocks, for *fmdry* = 0.20, switching time = 61 days, and 250 days of gas injection.

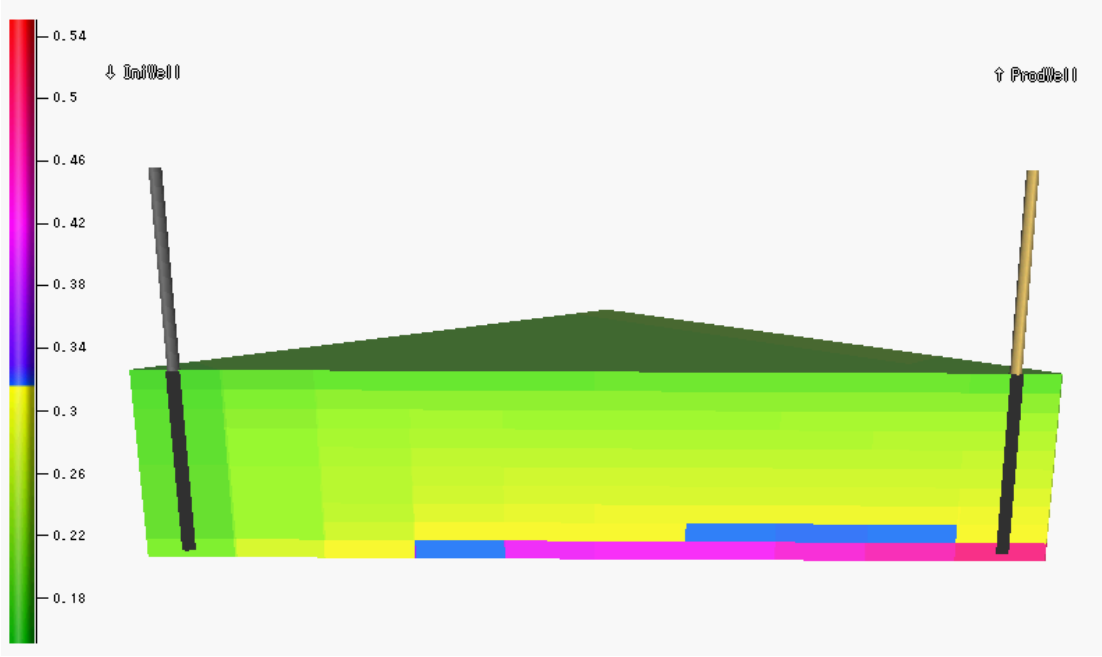

Figure 32: Water saturation in the gridblocks, for *fmdry* = 0.316, switching time = 61 days, and 250 days of gas injection.

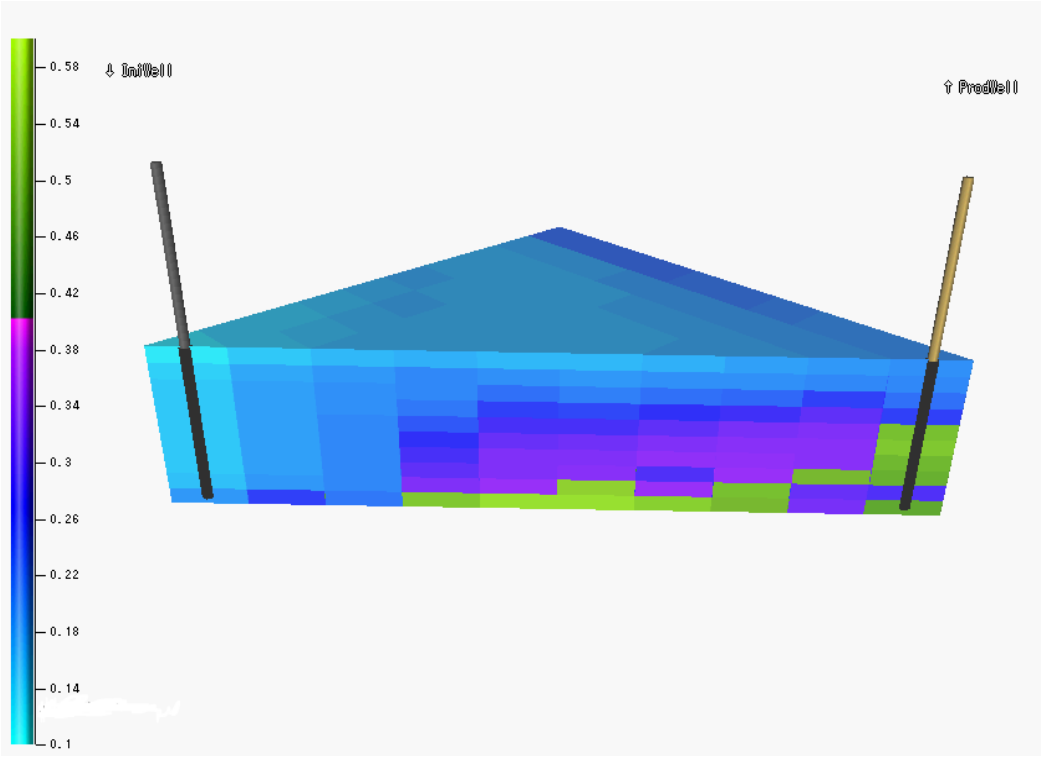

Figure 33: Oil saturation fm dry = 0.20, switching time = 61 days, and 250 days of gas injection.

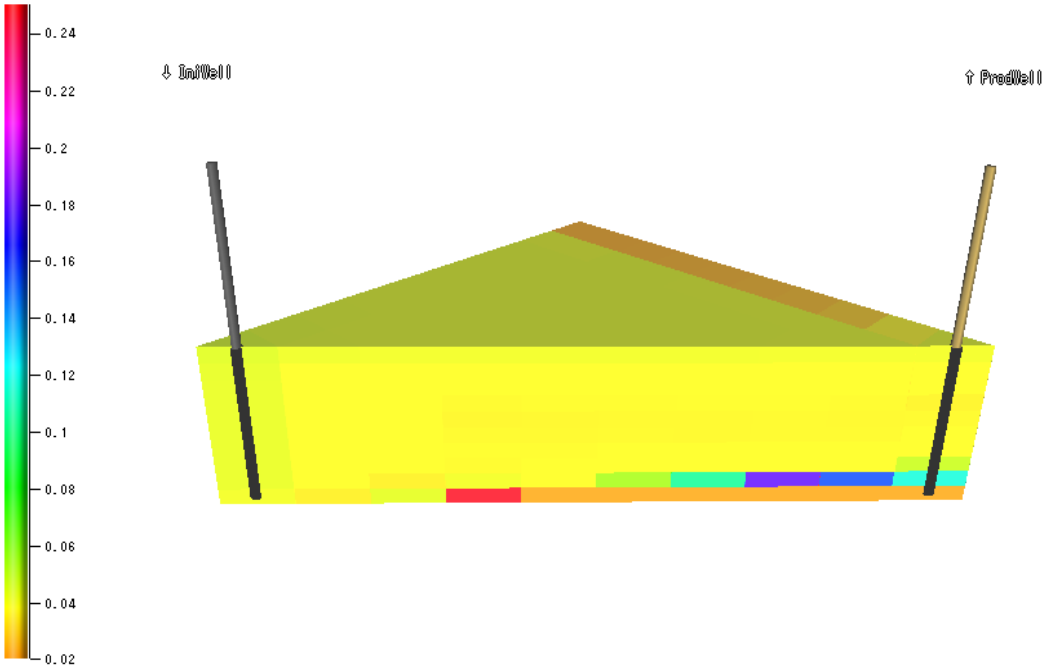

Figure 34: Gas viscosity for *fmdry* = 0.316, and switching time = 61 days.

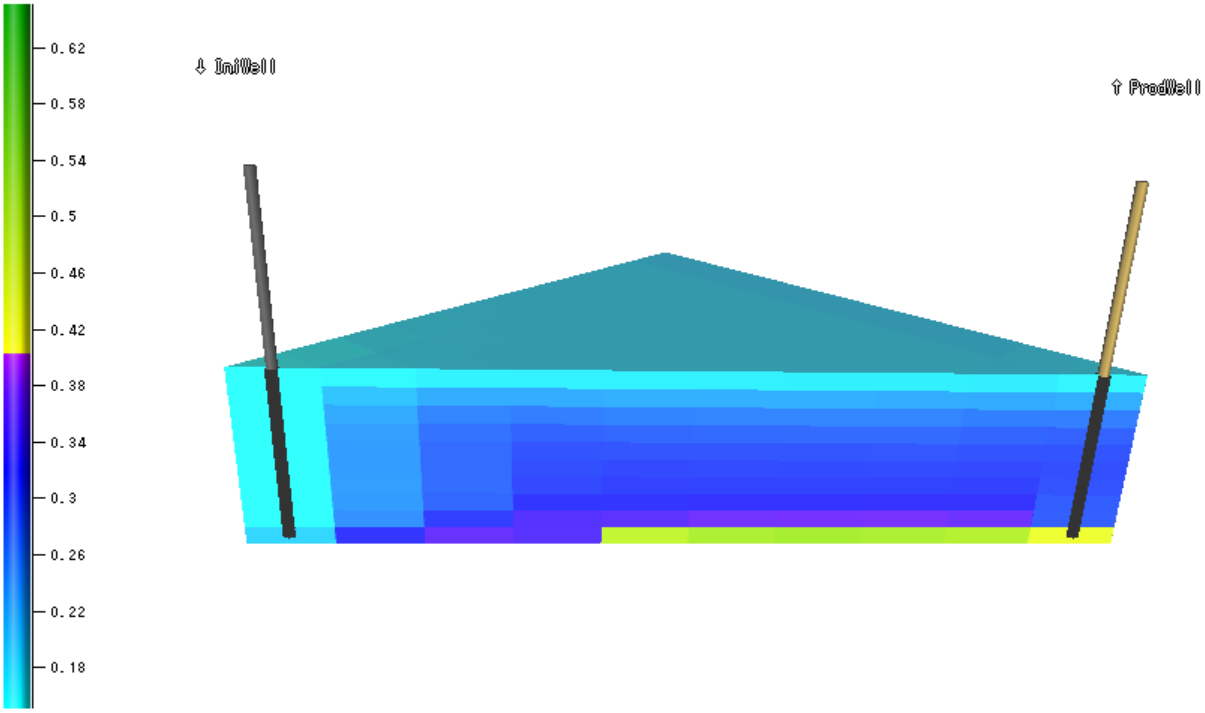

Figure 35: Oil saturation for *fmdry* = 0.316, and switching time = 61 days.

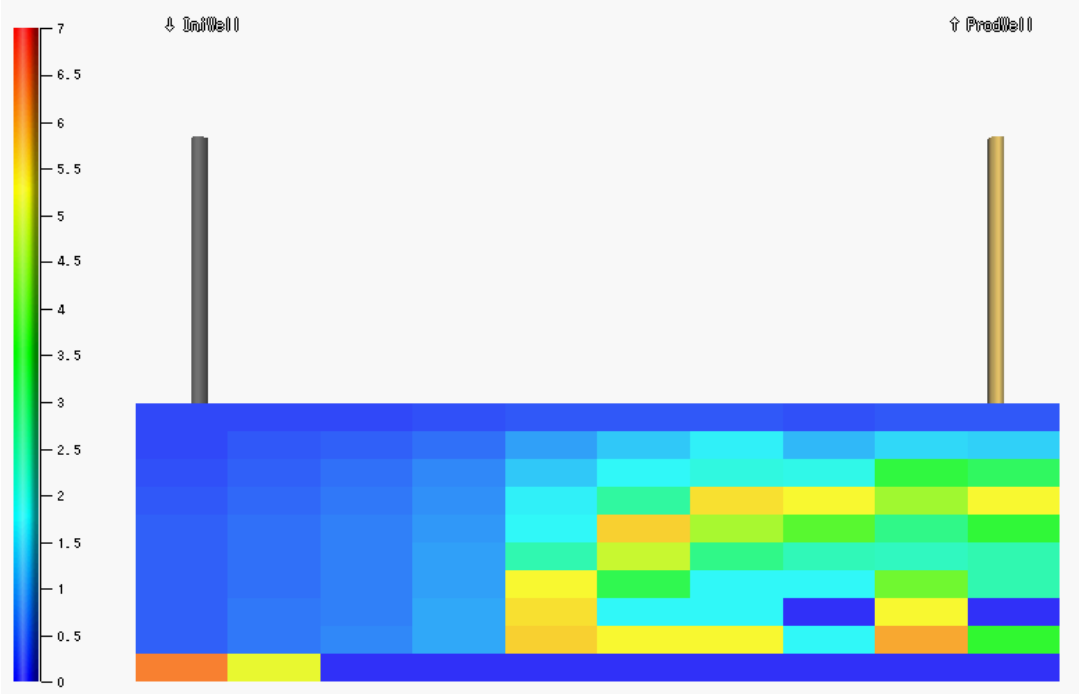

Figure 36: SAG process in a 2D reservoir, with dimensions 1mX100mX30m, and modeled with 1x10x10 gridblocks. This figure shows the gas viscosity (cP) at the end of the simulation. Switching time = 61 days, gas injection period = 250 days. The *fmdry* = 0.20, and the fm_oil = 0.40.

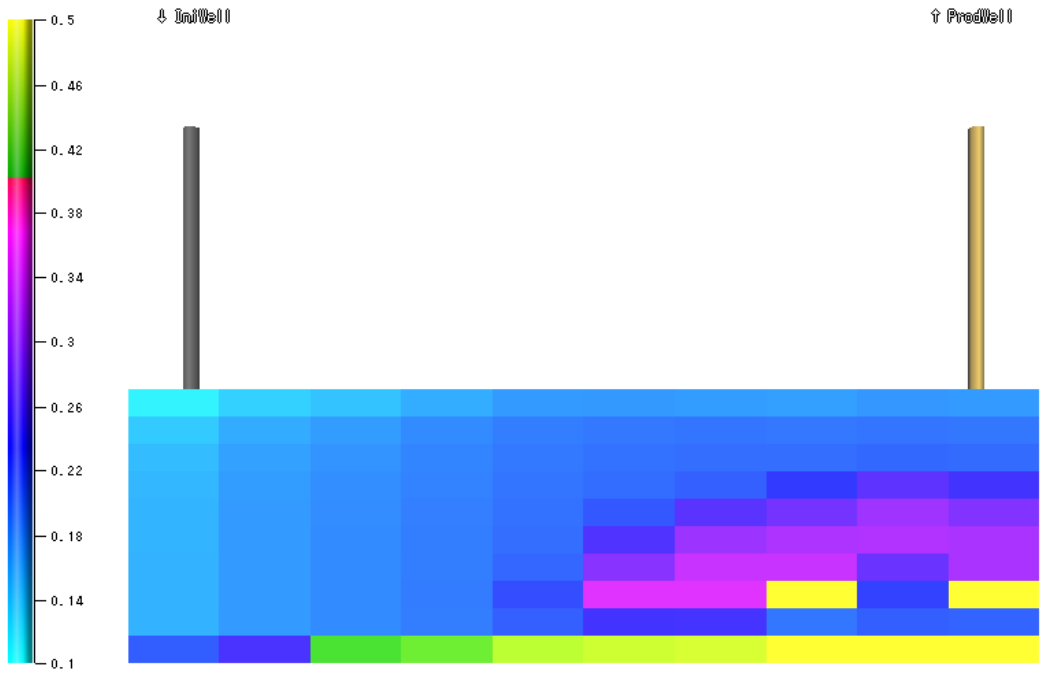

Figure 37: SAG process in a 2D reservoir, with dimensions 1mX100mX30m, and modeled with 1x10x10 gridblocks. This figure shows the oil saturation at the end of the simulation. Switching time = 61 days, gas injection period = 250 days. The *fmdry* = 0.20, and the fm_oil = 0.40.

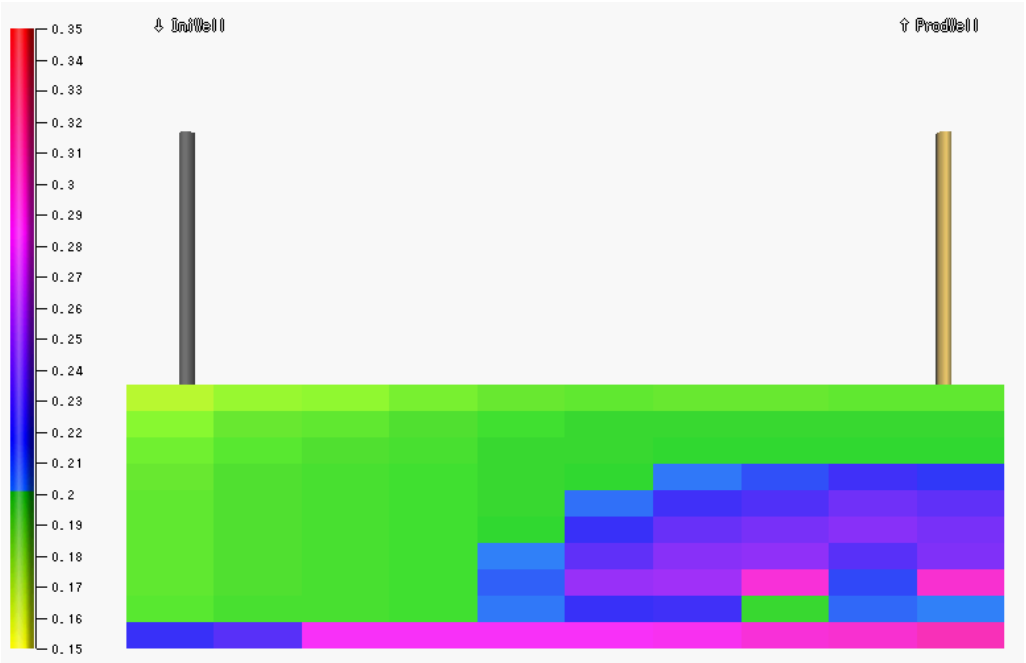

Figure 38: SAG process in a 2D reservoir, with dimensions 1mX100mX30m, and modeled with 1x10x10 gridblocks. This figure shows the water saturation at the end of the simulation. Switching time = 61 days, gas injection period = 250 days. The *fmdry* = 0.20, and the fm_oil = 0.40.

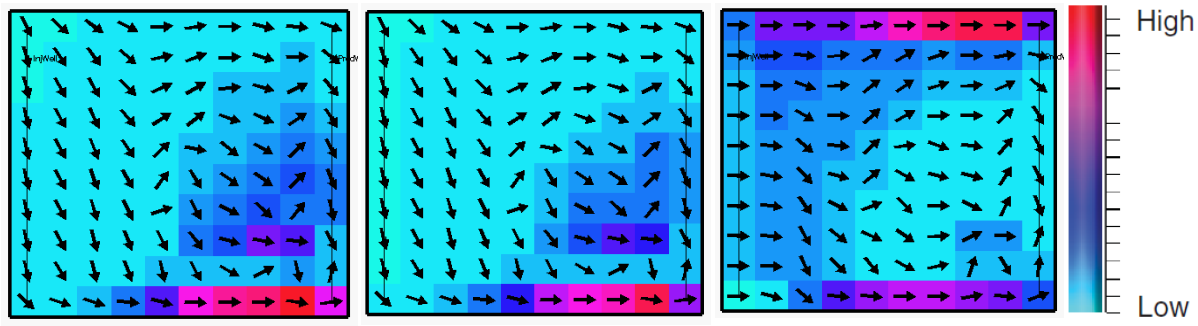

Water volume flux | Oil volume flux | Gas volume flux | Relative volume flux scale

Figure 39: SAG process in a 2D reservoir, with dimensions 1mX100mX30m, and modeled with 1x10x10 gridblocks. These figures show the net volume fluxes of the phases between the gridblocks at reservoir conditions at the end of the simulation. Switching time = 61 days, gas injection period = 250 days. The *fmdry* = 0.20, and the fm_oil = 0.40.

3.3. Conclusions and suggestions

3.3.1. Conclusions on simulations

- Cumulative oil production drops proportionally with the cumulative gas injection if insufficient surfactant is injected for the foam front to push the oil bank to reach the producer.
- Injecting enough surfactant into the reservoir for the foam front to push the oil bank to the producer, will significantly reduce the ratio of cumulative gas injection to cumulative oil production (up to a factor 20 in this report).
- Sufficient surfactant must be injected into the reservoir for foam to have a beneficial impact on the cumulative oil production.
- The maximum cumulative oil production is realized when enough surfactant is injected for the maximum MRF to be reached in every gridblock through which gas travels.
- The effect of the foam on the cumulative oil production and cumulative gas injection is less significant if the foam loses its stability at higher water saturations.
- In gridblocks where the oil saturation is higher than the threshold value above which foam is unstable, gas flows upward in the reservoir due to gravity, and pushes down oil and water. This results in oil and water accumulating at the bottom of the reservoir, and gas at the top of the reservoir. Due to the high oil saturation at the bottom of the reservoir, it can be that foam is unstable there and will override the oil bank at the bottom of the reservoir. The water saturation goes below the threshold value for stable foam at the top of the reservoir, and therefore gas will override foam.

3.3.2. Suggestions for future research

- Perform simulations with an *fmoil* that is higher than the oil saturations found in the reservoir, to further investigate the impact of the density and viscosity of oil.
- Perform simulations in finer grids to investigate the impact of possible fingering.
- Perform simulations for lower gas densities, to further investigate the impact of gravity on foam front stability and foam propagation.

References

1. Orr, F.M., *Theory of gas injection processes*. 2007: Tie-Line Publications Copenhagen.
2. Simjoo, M., *Immiscible Foam For Enhancing Oil Recovery*, in *Petroleum Engineering*. 2012, Delft University of Technology: Delft. p. 187.
3. Lake, L.W., *Enhanced oil recovery*. 1989.
4. Koval, E., *A method for predicting the performance of unstable miscible displacement in heterogeneous media.* Old SPE Journal, 1963. **3**(2): p. 145-154.
5. Rossen, W. and C. Van Duijn, *Gravity segregation in steady-state horizontal flow in homogeneous reservoirs*. Journal of Petroleum Science and Engineering, 2004. **43**(1): p. 99-111.
6. Waggoner, J., J. Castillo, and L. Lake, *Simulation of EOR processes in stochastically generated permeable media.* SPE formation evaluation, 1992. **7**(2): p. 173-180.
7. Hirasaki, G. and J. Lawson, *Mechanisms of foam flow in porous media: apparent viscosity in smooth capillaries.* Old SPE Journal, 1985. **25**(2): p. 176-190.
8. Suffridge, F.E., K.T. Raterman, and G.C. Russell, *Foam Performance Under Reservoir Conditions*, in *SPE Annual Technical Conference and Exhibition*. 1989, 1989 Copyright 1989, Society of Petroleum Engineers, Inc.: San Antonio, Texas.
9. Farajzadeh, R., A. Andrianov, and P.L.J. Zitha, *Foam Assisted Enhanced Oil Recovery at Miscible and Immiscible Conditions*, in *Kuwait International Petroleum Conference and Exhibition*. 2009, Society of Petroleum Engineers: Kuwait City, Kuwait.
10. Hirasaki, G., *The steam-foam process*. Journal of Petroleum Technology, 1989. **41**(5): p. 449-456.
11. Guo, H., et al. *A novel alkaline-surfactant-foam EOR process*. in *SPE Enhanced Oil Recovery Conference*. 2011.
12. Li, R., et al., *Foam mobility control for surfactant enhanced oil recovery.* SPE Journal, 2010. **15**(4): p. 928-942.
13. Patzek, T., *Field applications of steam foam for mobility improvement and profile control.* SPE Reservoir Engineering, 1996. **11**(2): p. 79-86.
14. Weaire, D.L. and S. Hutzler, *The physics of foams*. 1999: Oxford University Press.
15. Katgert, G., *Flow of Foams*. 2008, Universiteit Leiden: Leiden. p. 141.
16. Farajzadeh, R., et al., *Foam-oil interaction in porous media: Implications for foam assisted enhanced oil recovery.* Advances in Colloid and Interface Science, 2012. **183-184**(0): p. 1-13.
17. Jensen, J.A. and F. Friedmann, *Physical and Chemical Effects of an Oil Phase on the Propagation of Foam in Porous Media*, in *SPE California Regional Meeting*. 1987, Society of Petroleum Engineers Ventura, California.
18. Bond, D.C. and O.C. Holbrook, *Gas drive oil recovery process*. 1958: United States of America. p. 3.
19. Skauge, A., et al., *Foam-Assisted WAG: Experience from the Snorre Field*, in *SPE/DOE Improved Oil Recovery Symposium*. 2002, Copyright 2002, Society of Petroleum Engineers Inc.: Tulsa, Oklahoma.
20. Surguchev, L.M. and J.E. Hanssen, *Foam Application in North Sea Reservoirs, I: Design and Technical Support of Field Trials*, in *SPE/DOE Improved Oil Recovery Symposium*. 1996, 1996 Copyright 1996, Society of Petroleum Engineers, Inc.: Tulsa, Oklahoma.
21. Andrianov, A., et al., *Immiscible Foam for Enhancing Oil Recovery: Bulk and Porous Media Experiments.* Industrial & Engineering Chemistry Research, 2012. **51**(5): p. 2214-2226.
22. Schramm, L.L., A.T. Turta, and J.J. Novosad, *Microvisual and Coreflood Studies of Foam Interactions With a Light Crude Oil.* SPE Reservoir Engineering, 1993. **8**(3): p. 201-206.

23. Mannhardt, K., J.J. Novosad, and L.L. Schramm, *Foam/Oil Interations at Reservoir Conditions*, in *SPE/DOE Improved Oil Recovery Symposium*. 1998, Society of Petroleum Engineers: Tulsa, Oklahoma, USA.
24. Vikingstad, A.K. and M.G. Aarra, *Comparing the static and dynamic foam properties of a fluorinated and an alpha olefin sulfonate surfactant.* Journal of Petroleum Science and Engineering, 2009. **65**(1-2): p. 105-111.
25. Minssieux, L., *Oil Displacement by Foams in Relation to Their Physical Properties in Porous Media* Journal of Petroleum Technology, 1974. **26**(1): p. 100-108.
26. Mannhardt, K. and I. Svorstol, *Effect of oil saturation on foam propagation in Snorre reservoir core.* Journal of Petroleum Science and Engineering, 1999. **23**(3-4): p. 189-200.
27. Nikolov, A.D., et al., *The Effect of Oil on Foam Stability: Mechanisms and Implications for Oil Displacement by Foam in Porous Media*, in *SPE Annual Technical Conference and Exhibition*. 1986, 1986 Copyright 1986, Society of Petroleum Engineers: New Orleans, Louisiana.
28. Vikingstad, A.K., M.G. Aarra, and A. Skauge, *Effect of surfactant structure on foam-oil interactions: Comparing fluorinated surfactant and alpha olefin sulfonate in static foam tests.* Colloids and Surfaces A: Physicochemical and Engineering Aspects, 2006. **279**(1-3): p. 105-112.
29. Schramm, L.L., E.N. Stasiuk, and D.G. Marangoni, *Surfactants and their applications.* Annual Reports Section "C" (Physical Chemistry), 2003. **99**(0): p. 3-48.
30. Attwood, D. and A.T. Florence, *FASTtrack: Physical Pharmacy*. 2012: Pharmaceutical Press.
31. Kornev, K.G., A.V. Neimark, and A.N. Rozhkov, *Foam in porous media: thermodynamic and hydrodynamic peculiarities.* Advances in Colloid and Interface Science, 1999. **82**(1-3): p. 127-187.
32. Stevenson, P., *Foam engineering: fundamentals and applications*. 2012, Chichester: John Wiley & Sons.
33. Bergeron, V., *Disjoining Pressures and Film Stability of Alkyltrimethylammonium Bromide Foam Films.* Langmuir, 1997. **13**(13): p. 3474-3482.
34. Saint-Jalmes, A., M. Vera, and D. Durian, *Uniform foam production by turbulent mixing: new results on free drainage vs. liquid content.* The European Physical Journal B-Condensed Matter and Complex Systems, 1999. **12**(1): p. 67-73.
35. Carey, E. and C. Stubenrauch, *Free drainage of aqueous foams stabilized by mixtures of a non-ionic (C12DMPO) and an ionic (C12TAB) surfactant.* Colloids and Surfaces A: Physicochemical and Engineering Aspects, 2013. **419**(0): p. 7-14.
36. Hilgenfeldt, S., S.A. Koehler, and H.A. Stone, *Dynamics of coarsening foams: accelerated and self-limiting drainage.* Physical review letters, 2001. **86**(20): p. 4704.
37. Vikingstad, A.K., et al., *Foam-oil interactions analyzed by static foam tests.* Colloids and surfaces. A, Physicochemical and engineering aspects, 2005. **260**(1-3): p. 189-198.
38. Kuhlman, M.I., *Visualizing the effect of light oil on Co[2] foams.* Journal of Petroleum Technology, 1990. **42**: p. 902-908.
39. Zhu, T., et al., *Foams for Mobility Control and Improved Sweep Efficiency in Gas Flooding*, in *SPE/DOE Improved Oil Recovery Symposium*. 1998, 1998 Copyright 1998, Society of Petroleum Engineers, Inc.: Tulsa, Oklahoma.
40. Denkov, N.D., *Mechanisms of Foam Destruction by Oil-Based Antifoams.* Langmuir, 2004. **20**(22): p. 9463-9505.
41. Lee, J., A. Nikolov, and D. Wasan, *Stability of Aqueous Foams in the Presence of Oil: On the Importance of Dispersed vs Solubilized Oil.* Industrial & Engineering Chemistry Research, 2013. **52**(1): p. 66-72.

42. Schramm, L.L. and J.J. Novosad, *Micro-visualization of foam interactions with a crude oil.* Colloids and Surfaces, 1990. **46**(1): p. 21-43.
43. Schramm, L.L. and J.J. Novosad, *The destabilization of foams for improved oil recovery by crude oils: Effect of the nature of the oil.* Journal of Petroleum Science and Engineering, 1992. **7**(1-2): p. 77-90.
44. Dalland, M., J.E. Hanssen, and T.S.m. Kristiansen, *Oil interaction with foams under static and flowing conditions in porous media.* Colloids and Surfaces A: Physicochemical and Engineering Aspects, 1994. **82**(2): p. 129-140.
45. Aronson, A.S., et al., *The influence of disjoining pressure on foam stability and flow in porous media.* Colloids and Surfaces A: Physicochemical and Engineering Aspects, 1994. **83**(2): p. 109-120.
46. Rolo, L.I., et al., *Surface Tension of Heptane, Decane, Hexadecane, Eicosane, and Some of Their Binary Mixtures.* Journal of Chemical & Engineering Data, 2002. **47**(6): p. 1442-1445.
47. Hardy, R.C., *Viscosity of n-Hexadecane.* Journal of Research of the National Bureau of Standards, 1958. **61**(5): p. 433.
48. Pubchem. *n-hexadecane - Compound Summary.* 2013; Available from: http://pubchem.ncbi.nlm.nih.gov/summary/summary.cgi?q=all&cid=11006#ec.
49. Du Nouy, P.L., *A new apparatus for measuring surface tension.* The Journal of general physiology, 1919. **1**(5): p. 521.
50. Carrier, V. and A. Colin, *Anisotropy of Draining Foams.* Langmuir, 2002. **18**(20): p. 7564-7570.
51. Saint-Jalmes, A. and D. Langevin, *Time evolution of aqueous foams: drainage and coarsening.* Journal of Physics: Condensed Matter, 2002. **14**(40): p. 9397.
52. Zhu, B.Y. and M.J. Rosen, *Synergism in binary mixtures of surfactants: IV. Effectiveness of surface tension reduction.* Journal of Colloid and Interface Science, 1984. **99**(2): p. 435-442.
53. Micheau, C., et al., *Specific Salt and pH Effects on Foam Film of a pH Sensitive Surfactant.* Langmuir, 2013. **29**(27): p. 8472-8481.
54. Garrett, P.R., *Preliminary considerations concerning the stability of a liquid heterogeneity in a plane-parallel liquid film.* Journal of Colloid and Interface Science, 1980. **76**(2): p. 587-590.
55. Harkins, W.D. and A. Feldman, *The spreading of liquids and the spreading coefficient.* American Chemical Journal, 1922.
56. Chen, S.J., D.F. Evans, and B.W. Ninham, *Properties and structure of three-component ionic microemulsions.* The Journal of Physical Chemistry, 1984. **88**(8): p. 1631-1634.
57. Kunieda, H., et al., *The formation of gel-emulsions in a water/nonionic surfactant/oil system.* Colloids and Surfaces, 1987. **24**(2-3): p. 225-237.
58. Kabalnov, A.S. and E.D. Shchukin, *Ostwald ripening theory: applications to fluorocarbon emulsion stability.* Advances in Colloid and Interface Science, 1992. **38**(0): p. 69-97.
59. Weiss, J., J.N. Coupland, and D.J. McClements, *Solubilization of Hydrocarbon Emulsion Droplets Suspended in Nonionic Surfactant Micelle Solutions.* The Journal of Physical Chemistry, 1996. **100**(3): p. 1066-1071.
60. Zanganeh, M.N. and W. Rossen, *Optimization of Foam Enhanced Oil Recovery: Balancing Sweep and Injectivity.* SPE Reservoir Evaluation & Engineering, 2013. **16**(1): p. pp. 51-59.
61. Peaceman, D.W., *Improved Treatment of Dispersion in Numerical Calculation of Multidimensional Miscible Displacement.* 1966.
62. Baker, L.E., *Three-Phase Relative Permeability Correlations*, in *SPE Enhanced Oil Recovery Symposium*. 1988, 1988: Tulsa, Oklahoma.

63. Surguchev, L., et al. *Simulation of WAG and gas Injection with potential sweep improvement by application of foam*. in *8th European Symposium on Improved Oil Recovery*. 1995.
64. Cheng, L., et al., *Simulating Foam Processes at High and Low Foam Qualities*, in *SPE/DOE Improved Oil Recovery Symposium* 2000, Society of Petroleum Engineers: Tulsa, Oklahoma.
65. Khatib, Z.I., G.J. Hirasaki, and A.H. Falls, *Effects of Capillary Pressure on Coalescence and Phase Mobilities in Foams Flowing Through Porous Media.* SPE Reservoir Engineering, 1988. **3**(3): p. 919-926.
66. Rossen, W.R., Z.H. Zhou, and C.K. Mamun, *Modeling Foam Mobility in Porous Media.* SPE Advanced Technology Series, 1995. **3**(1): p. 146-153.
67. Zanganeh, M.N., *Simulation and Optimization of Foam EOR Processes*. 2011, Delft University of Technology: Delft. p. 198.

Appendix 1. Comparison plots

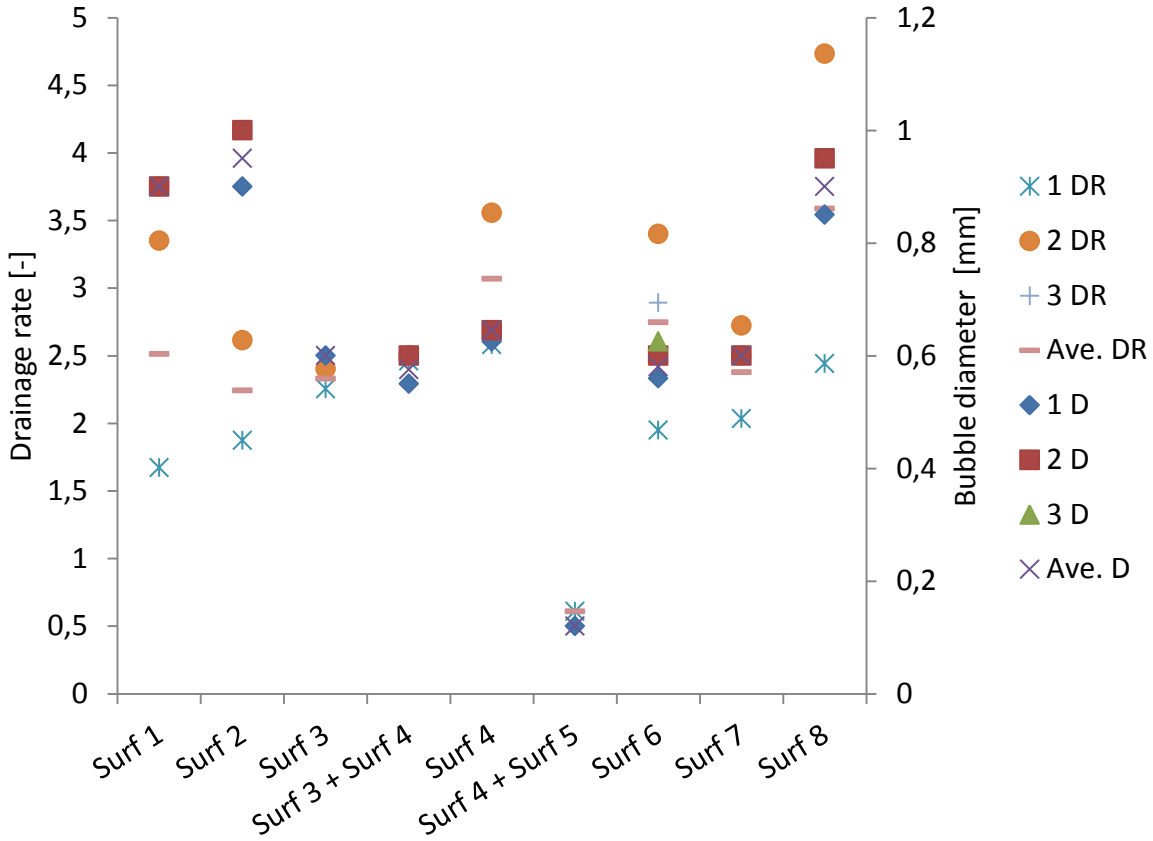

Figure 40: This figure shows the bubble diameters [mm] and the drainage rates [-] of the foams in absence of oil. Explanation of legend: the numbers denote the corresponding experiment, Ave. = average, DR = Drainage rate, D = Bubble diameter.

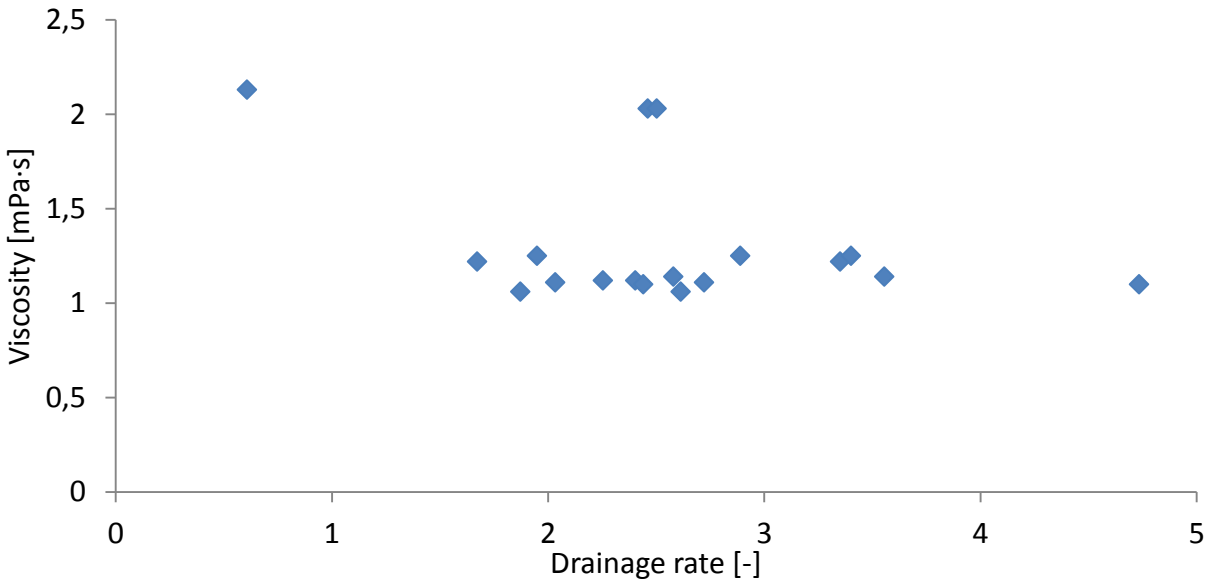

Figure 41: This figure shows a cross plot of the surface viscosities [mPa·s] and drainage rate of the foams in absence of oil. The surface viscosities were measured at a shear rate of 2 [s^{-1}].

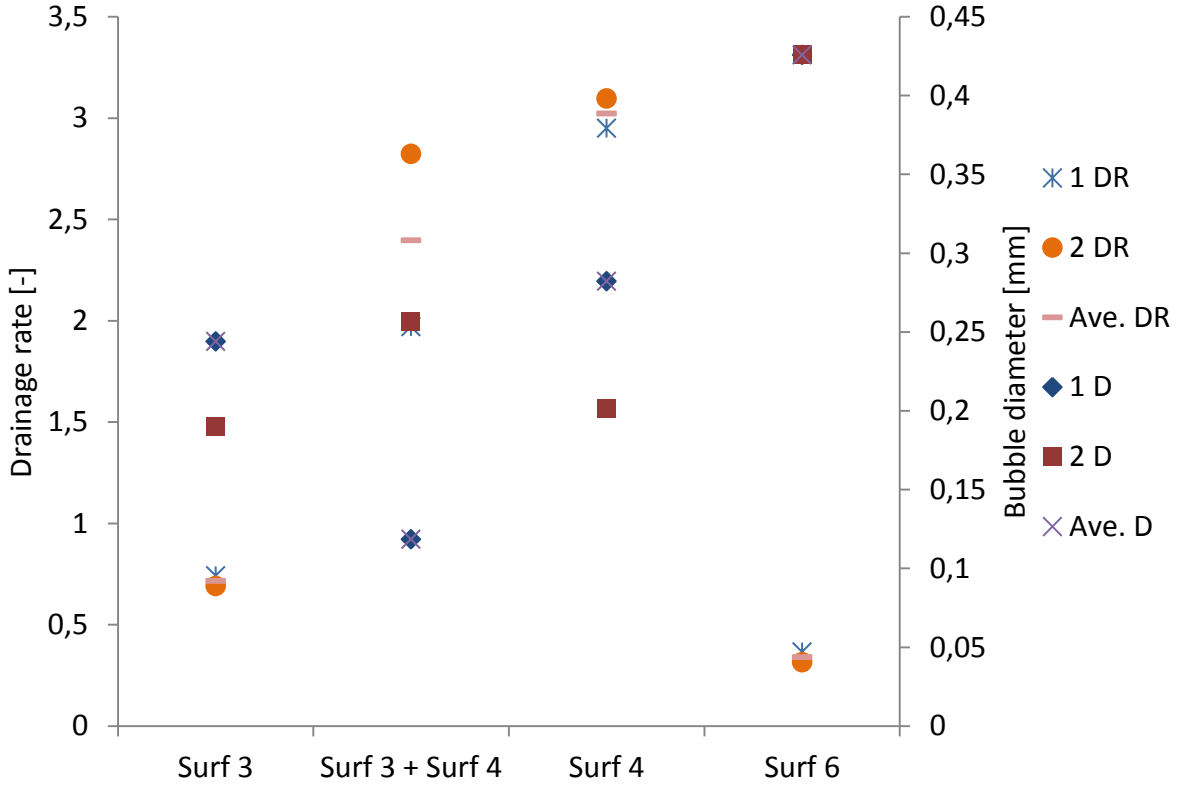

Figure 42: This figure shows the bubble diameters [mm] and the drainage rates [-] of the foams in presence of oil. Explanation of legend: the numbers denote the corresponding experiment, Ave. = average, DR = drainage rate, D = bubble diameter.

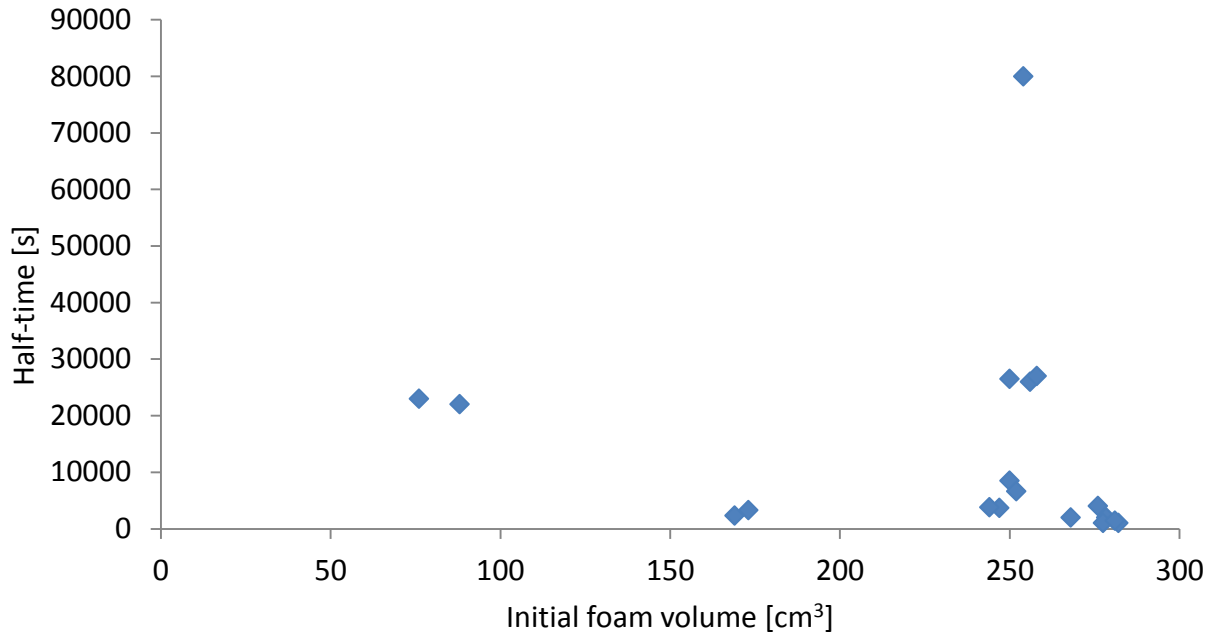

Figure 43: This figure shows a cross-plot of the half-times [s] and initial foam volumes [cm^3] of the foams in presence of oil.

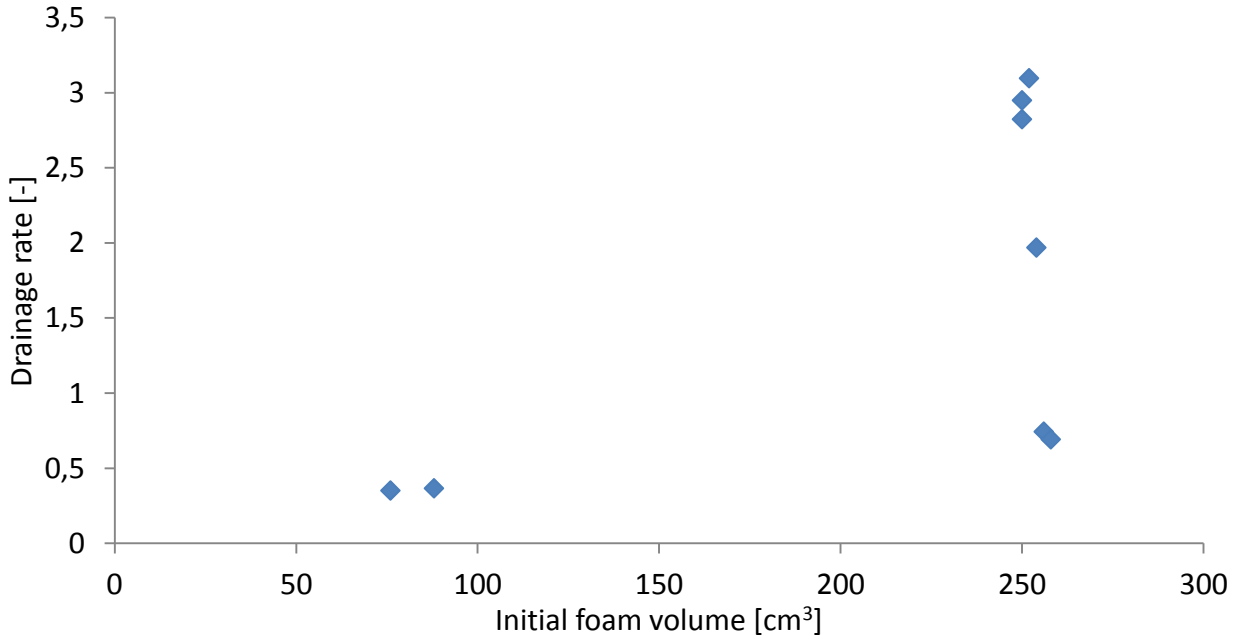

Figure 44: This figure shows a cross-plot of the drainage rates [-] and initial foam volumes [cm^3] of the foams in presence of oil.

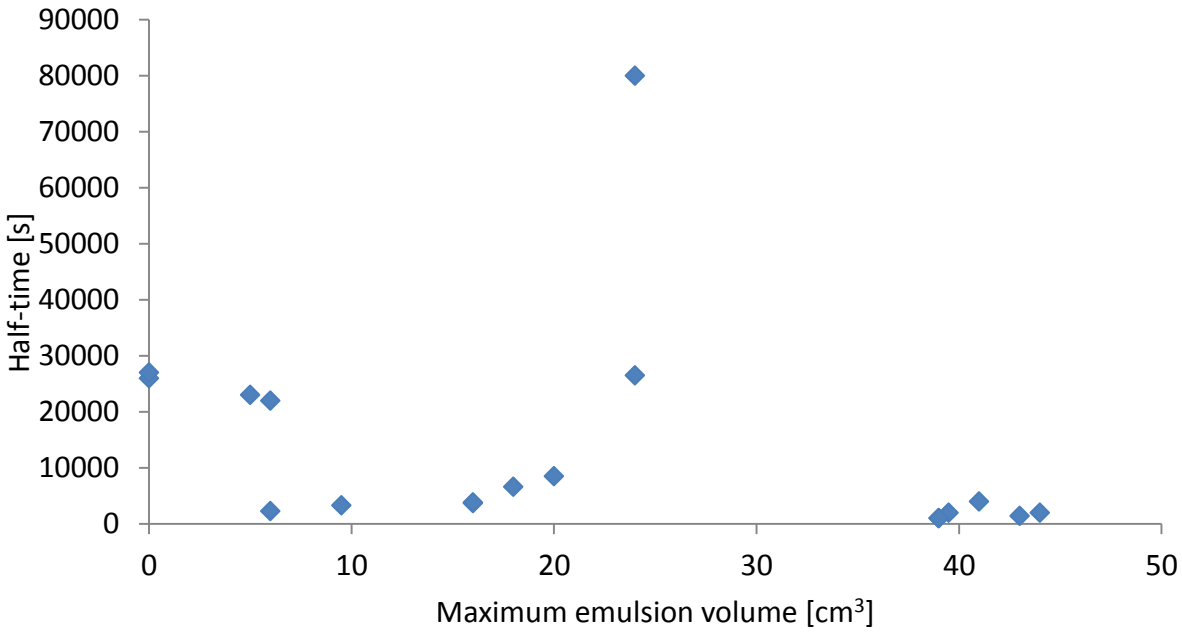

Figure 45: This figure shows a cross-plot of the half-times [s] and maximum emulsion volumes [cm^3] of the foams in presence of oil.

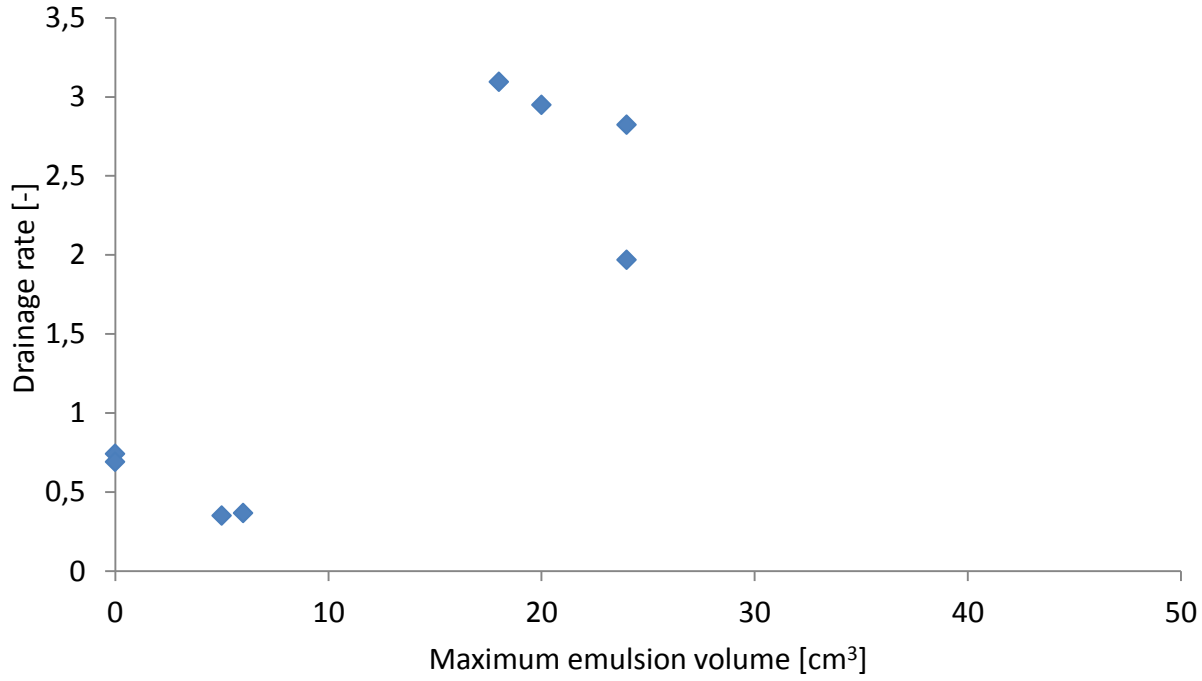

Figure 46: This figure shows a cross-plot of the drainage rates [-] and maximum emulsion volumes [cm^3] of the foams in presence of oil.

Appendix 2. Two-Phase and Three-Phase Relative-Permeability Models

For the two-phase water-oil system (S_g = 0), the relative permeabilities are given by **Eqs. (14)** and **(15)**. K_{rw}^0 is the end-point relative permeability of water and K_{row}^0 is the end-point relative permeability of oil. S_{orw} denotes the oil saturation residual to water flood. n_w and n_{ow} denote the water and oil Corey exponents.

$$\mathrm{k_{rwo}} = K_{rw}^0 \left(\frac{\mathrm{S_w} - \mathrm{S_{wc}}}{1 - \mathrm{S_{wir}} - \mathrm{S_{orw}}} \right)^{\mathrm{n_w}} \quad \textbf{(14)}$$

$$k_{row} = K_{row}^0 \left(\frac{1 - S_w - S_{orw}}{1 - S_{wir} - S_{orw}} \right)^{n_{ow}} \quad \textbf{(15)}$$

For the two-phase gas-oil system (S_w=S_{wr}), the relative permeabilities are given by Eqs. **(16)** and **(17)**. $K_{rg}^0$is the end-point relative permeability of gas and K_{rog}^0 is the end-point relative permeability of oil. S_{org} denotes the oil saturation, residual to gas flood. n_g and n_{og} denote the water and oil Corey exponents.

$$k_{rgo} = K_{rg}^0 \left(\frac{S_g - S_{gr}}{1 - S_{wir} - S_{gr} - S_{org}} \right)^{n_g} \quad \textbf{(16)}$$

$$k_{rog} = K_{rog}^0 \left(\frac{1 - S_g - S_{org} - S_{wir}}{1 - S_{wir} - S_{gr} - S_{org}} \right)^{n_{og}} \quad \textbf{(17)}$$

Because irreducible water is present in the gas-oil relative-permeability simulation experiment, it is important that the two-phase tables are consistent. Therefore it must be that $k_{row}(S_w = S_{wir}) = k_{rog}(S_g = 0 \text{ and } S_w = S_{wir})$, and thus K_{row}^0 must be equal to K_{rog}^0. k_{ro} is zero for oil saturation residual to the displacing fluid, i.e. $k_{row}(S_w = 1 - S_{orw}) = k_{rog}(S_g = 1 - S_{wir}) = 0$.

The three-phase relative permeabilities are calculated according to the saturation-weighted model, see Eq. **(18)**, **(19)**, and **(20)**, for more information see Baker [62].

$$\mathrm{k_{ro}} = \frac{(\mathrm{S_w} - \mathrm{S_{wc}})\mathrm{k_{row}} + (\mathrm{S_g} - \mathrm{S_{gr}})\mathrm{k_{rog}}}{(\mathrm{S_w} - \mathrm{S_{wc}}) + (\mathrm{S_g} - \mathrm{S_{gr}})} \quad \textbf{(18)}$$

$$\mathrm{k_{rw}} = \frac{(\mathrm{S_o} - \mathrm{S_{or}})\mathrm{k_{rwo}} + (\mathrm{S_g} - \mathrm{S_{gr}})\mathrm{k_{rwg}}}{(\mathrm{S_o} - \mathrm{S_{or}}) + (\mathrm{S_g} - \mathrm{S_{gr}})} \quad \textbf{(19)}$$

$$\mathrm{k_{rg}} = \frac{(\mathrm{S_o} - \mathrm{S_{or}})\mathrm{k_{rgo}} + (\mathrm{S_g} - \mathrm{S_{gr}})\mathrm{k_{rgw}}}{(\mathrm{S_o} - \mathrm{S_{or}}) + (\mathrm{S_w} - \mathrm{S_{wc}})} \quad \textbf{(20)}$$

Appendix 3. Model parameters

The parameters of the relative permeability model and foam model are summarized in **Table 8**; specifically it gives the values for the residual saturations, the values of the parameters for the relative-permeability model, and foam model. These values are used to calculate the two-phase relative permeability in the absence of foam, for each phase α. The reservoir properties, simulation parameters, and well constraints are summarized in **Table 9**. The fluid properties at reservoir conditions are summarized in **Table 10**.

Appendix 4. Foam Model

Eq. 13 describes how the foam modifies the gas mobility; the factors F_o, F_s, and F_w are defined below. Foam collapses if the water saturation is below the threshold value *(fmdry)* [65, 66]; F_w describes the foam strength as a function of water saturation, see **Eq.(21)**. This relationship is adapted from Namdar Zanganeh [67].

$$F_w = \frac{arctan[epdry(S_w - fmdry)]}{\pi} - \frac{arctan[epdry(S_{wir} - fmdry)]}{\pi} \quad \textbf{(21)}$$

The relationship of foam strength and oil saturation is adapted from STARS 2007, see **Eq.(22)**.

$$F_o = \begin{cases} 1 & S_o < floil \\ \left(\dfrac{fmoil - S_o}{fmoil - floil}\right)^{epoil} & floil \le S_o \le fmoil \\ 0 & fmoil \le S_o \le (1 - S_{wr}) \end{cases} \quad \textbf{(22)}$$

The relationship of foam strength and surfactant concentration in the aqueous phase is given in **Eq.(23)**.The critical surfactant concentration (C_s^*) is 0.0012 kg/kg, and this is half the concentration in the injected water.

$$\begin{aligned} F_s &= Cs/Cs^* \quad Cs < Cs^* \\ F_s &= 1 \quad\quad Cs > Cs^* \end{aligned} \quad \textbf{(23)}$$